Negative Regulation of Autophagy by UBA6-BIRC6–Mediated Ubiquitination of LC3

Rui Jia[1] and Juan S. Bonifacino[1, *]

[1]Cell Biology and Neurobiology Branch

Eunice Kennedy Shriver National Institute of Child Health and Human Development,

National Institutes of Health, Bethesda, Maryland, 20892, USA

[*]Correspondence: juan.bonifacino@nih.gov

T: 301-496-6368; F: 301-402-9319

Abstract

Although the process of autophagy has been extensively studied, the mechanisms that regulate it remain insufficiently understood. The ability to manipulate autophagy is important not only for addressing fundamental biological questions, but also for its possible application to the treatment of various human diseases. To identify novel regulators of autophagy, we performed a whole-genome CRISPR/Cas9 knockout screen in H4 human neuroblastoma cells gene-edited to express the endogenous autophagy effector LC3B fused to a tandem of GFP and mCherry. Using this methodology, we identified the ubiquitin-activating (E1) enzyme UBA6 and the hybrid ubiquitin-conjugating (E2)/ubiquitin-ligase (E3) enzyme BIRC6 as important autophagy regulators. We found that these two enzymes cooperate to monoubiquitinate LC3B on lysine-51, targeting it for degradation by the proteasome. Knockout of UBA6 or BIRC6 increased the levels of LC3B as well as autophagic flux under conditions of nutrient deprivation or protein synthesis inhibition. Moreover, depletion of UBA6 or BIRC6 KO decreased the formation of aggresome-like induced structures in H4 cells, and aggregates of an α-synuclein mutant in the axon of rat hippocampal neurons. These findings demonstrate that UBA6 and BIRC6 negatively regulate autophagy by limiting the availability of LC3B, possibly to prevent the deleterious effects of excessive autophagy. Inhibition of UBA6 or BIRC6, on the other hand, could be used to enhance autophagic clearance of protein aggregates in neurodegenerative disorders.

Introduction

Macroautophagy (herein referred to as autophagy) is a catabolic process involving the engulfment of cytoplasmic materials into double-membraned autophagosomes that subsequently fuse with lysosomes to form autolysosomes, where the materials are degraded by acid hydrolases [1] [2]. Autophagy substrates include abnormal particles such as protein aggregates, damaged organelles and intracellular pathogens. Autophagy is also involved in the degradation of normal cellular constituents for survival under conditions of nutrient restriction or other stresses. Through these functions, autophagy plays crucial roles in the maintenance of cellular homeostasis. Defective autophagy contributes to the pathogenesis of various disorders, including neurodegeneration, cancer, cardiomyopathies and infectious diseases [2] [3].

The mechanism of autophagy involves multiple steps, including induction by cellular signals, phagophore formation and elongation, substrate engulfment, autophagosome formation, and autophagosome-lysosome fusion [1] [2]. Key components of the autophagy machinery are members of the Atg8 family of ubiquitin (Ub)-like proteins (LC3A, LC3B, LC3C, GABARAP, GABARAPL1 and GABARAPL2 in mammals), which play roles in autophagosome formation and autophagosome-lysosome fusion [4] [5]. The best studied member of this family is LC3B (product of the MAP1LC3B gene), which undergoes conversion from a soluble, cytosolic form (LC3B-I) to a phosphatidylethanolamine (PE)-conjugated, membrane-bound form (LC3B-II) [6]. LC3B-II subsequently interacts with the LC3-interacting region (LIR) of various cargo receptors to capture autophagic cargos into forming autophagosomes [4] [5]. Among these receptors are cytosolic proteins such as SQSTM1 (p62), NBR1, NDP52, OPTN and TAX1BP1, which bind polyubiquitinated cargos via their Ub-binding domains [4] [5]. Other cargo receptors are anchored to the autophagy cargos via their transmembrane domains, as is the case for BNIP3, NIX and FUNDC1 in mitochondrial autophagy (mitophagy) [4] [5], and RTN3, SEC62, CCPG1, FAM134B and TEX264 in endoplasmic reticulum (ER) autophagy (ER-

phagy) [7] [8] [9] [10] [11] [12]. After fusion of autophagosomes with lysosomes, the autophagy cargos, together with the Atg8-family proteins and cargo receptors, are degraded in lysosomes [13] [14].

The autophagy machinery is regulated by post-translational modifications such as phosphorylation and ubiquitination. Several kinases have been implicated in positive or negative regulation of autophagy. As an example of positive regulation, the unc-51-like autophagy-activating kinase 1 (ULK1) phosphorylates the VPS34 [15], BECN1 [16] and ATG14L1 [17] components of the class III PI3K complex, which subsequently catalyzes the conversion of phosphatidylinositol (PI) to phosphatidylinositol 3-phosphate [PI(3)P], thus triggering phagophore formation. ULK1 itself is activated by phosphorylation on Ser-317, Ser-555 and Ser-777 catalyzed by AMP-activated protein kinase (AMPK) [18] [19]. On the other hand, the mechanistic target of rapamycin (mTOR) complex-1 (mTORC1) kinase negatively regulates autophagy by phosphorylating ULK1 on Ser-757, and thus preventing the interaction of ULK1 with AMPK [19]. The mTORC1 kinase exerts an additional inhibitory effect on autophagy by phosphorylating the autophagy protein UVRAG, a modification that decreases autophagosome maturation and autophagosome-lysosome fusion [20].

Ubiquitination also plays positive and negative roles in autophagy. In fact, some of the kinases or kinase complexes that regulate autophagy are themselves targets of ubiquitination. For instance, ULK1 and BECN1 are positively regulated by polyubiquitination mediated by the Ub-ligase (E3) TRAF6 [21] [22]. Non-enzymatic components of the autophagy machinery can also be positively regulated by ubiquitination, as is the case for the polyubiquitination of OPTN by the E3 HACE1, which promotes assembly of OPTN with SQSTM1 and thus results in enhanced autophagic degradation [23]. An example of the negative effects of ubiquitination on autophagy is the activation of mTORC1 by TRAF6-mediated polyubiquitination of the catalytic mTOR subunit, with consequent inhibition of autophagy [24]. Furthermore, ULK1 and components of the class III PI3K complex are targeted for polyubiquitination and degradation

by the E3 Cul3-KLHL20 [25]. Finally, BECN1 is polyubiquitinated by the RNF216 and NEDD4 E3s, causing destabilization of the class III PI3K complex [26] [27].

Both phosphorylation and ubiquitination have been targeted for pharmacologic manipulation of autophagy. For example, inhibition of mTORC1 by the drugs rapamycin or torin1 [28] [29], or activation of AMPK by metformin [30], are widely used to stimulate autophagy. In contrast, inhibition of the class III PI3K complex by wortmannin, LY294002 or 3-methyladenine impairs autophagy [31] [32]. Finally, inhibition of USP10/13-mediated deubiquitination of BECN1 by spautin-1 causes destabilization and degradation of the class III PI3K complex, decreasing autophagy [33]. Autophagy stimulation has been proposed as a possible therapy for neurodegenerative disorders caused by accumulation of intracellular protein aggregates [33]. Autophagy inhibition, on the other hand, could be used to treat hyperproliferative disorders fueled by increased autophagy, as is the case for some cancers [34]. However, the involvement of known regulators of autophagy in other cellular processes has hampered efforts to exploit their pharmacologic activation or inhibition for clinical uses. Therefore, there is a need to identify additional autophagy regulators that could be targeted for therapeutic applications.

To identify additional autophagy regulators, we conducted a genome-wide CRISPR/Cas9 knockout (KO) screen using cells that were gene-edited to express endogenous LC3B tagged with tandem GFP and mCherry fluorescent proteins. This screen is based on the acid-induced quenching of GFP, but not mCherry, upon fusion of autophagosomes with lysosomes [35]. Mutant cells displaying higher GFP:mCherry fluorescence ratios were selected by fluorescence-activated cell sorting (FACS), and the mutated genes were identified by next-generation sequencing. The reliability of the screen was demonstrated by the identification of genes encoding virtually all core components of the autophagy machinery. In addition, we identified other candidates, among which were two ubiquitination-related proteins: the Ub-activating (E1) UBA6 and the hybrid Ub-conjugating/Ub-ligase (E2/E3) BIRC6 enzymes.

Further analyses showed that these enzymes mediate monoubiquitination of LC3B, marking it for degradation by the proteasome. KO of UBA6 or BIRC6 increased the levels of LC3B, and lessened the accumulation of aggresome-like induced structures (ALIS) in non-neuronal cells and α-synuclein aggregates in neurons. These findings thus identify UBA6 and BIRC6 as negative regulators of autophagy, whose inhibition could be used to enhance autophagy and thus prevent the accumulation of pathogenic protein aggregates.

Results

Identification of autophagy genes by CRISPR/Cas9 KO screening in human cells

This project was aimed at identifying novel autophagy genes in mammalian cells by taking advantage of the development of pooled CRISPR/Cas9 KO libraries for whole-genome phenotypic screens [36]. To this end, we developed an indicator cell line that enabled the selection of autophagy-defective cells by FACS. This cell line, named H4-tfLC3B, was made by gene-editing human neuroglioma H4 cells to express endogenous LC3B tagged at its N-terminus with tandem GFP and mCherry fluorescent proteins (designated GFP-mCherry-LC3B) (Figures S1A, S1B). The quenching of GFP, unlike mCherry, in the acidic pH of autolysosomes allows the use of GFP:mCherry ratio to monitor the delivery of GFP-mCherry-LC3B from neutral autophagosomes to acidic autolysosomes (referred to as "autophagy flux") [35]. Moreover, endogenous tagging avoids the overexpression artifacts caused by transfection of cells with plasmids encoding fluorescently tagged LC3B [35]. Live-cell imaging of H4-tfLC3B cells revealed puncta displaying both GFP and mCherry fluorescence (*i.e.*, autophagosomes), or only mCherry fluorescence (*i.e.*, autolysosomes) (Figure 1A). Treatment of these cells with the v-ATPase inhibitor bafilomycin A_1 increased the number of puncta containing GFP in addition to mCherry (Figure 1A), as well as the GFP:mCherry ratio in FACS analyses (seen as a displacement to the right in Figure 1B), consistent with the presence of quenched GFP in autolysosomes. In contrast, depletion of serum and amino acids from the medium (*i.e.*, nutrient deprivation) decreased the GFP:mCherry ratio detected by FACS (seen as a shift to the left in Figures 1C, S1C), as expected from the induction of autophagy under conditions of nutrient shortage [37]. Thus, the H4-tfLC3B cell line exhibited the expected responses to the inhibition or stimulation of autophagy.

H4-tfLC3 cells were mutated with the human GeCKO v2 lentiviral pooled library, containing 123,411 sgRNAs targeting 19,050 genes and 1,864 miRNAs [38]. FACS was used to

collect the top 1% of cells with increased GFP:mCherry ratio (Figure 1D). These cells were successively expanded and sorted an additional four rounds, resulting in an enrichment of cells with high GFP to mCherry ratio from 1.02% to 89.0% (Figures 1E, S1D). The genes that were mutated in these cells were identified by next-generation sequencing of the integrated sgRNAs (Figure 1D, Table S1). The enrichment of each gene in the sorted *vs.* unsorted population was calculated using the MAGeCK algorithm [39] (Figure 1F). Most of the top-ranked genes in this analysis corresponded to known components of the core autophagy machinery (Figure 1F, Table S2) [1], demonstrating the reliability of the screen. A number of previously reported autophagy regulators were also identified with lower but still significant scores; these included the MEF2BNB and SNAPIN subunits of BORC [40 41], C18orf8 [42], BECN1 [43], RAB1A [44], EPG5 [45] and CCZ1 [42] (Figure 1F, Table S2).

To confirm candidates from the primary screen, we constructed a secondary pooled CRISPR/Cas9 lentiviral library targeting the top 432 protein-coding genes , by combining the sgRNA sequences from two published CRISPR/Cas9 screens [36] [46] (Table S3). This secondary library excluded sgRNAs the top 20 autophagy genes, except the sgRNAs for ATG7 and VPS16 that were included as positive controls (Table S3). H4-tfLC3B cells were mutated by the secondary CRISPR/Cas9 library, and the cells with defective autophagy were selected by three rounds of FACS (Figures 2A, S2A), and analyzed by next-generation sequencing (Figure 2B, Tables S4, S5), as described above. Most of the genes exhibiting significant scores in this secondary screen were also known regulators of autophagy (Figure 2B). *UBA6*, however, stood out as a gene with relatively high scores in both the primary (Figure 1F) and secondary screens (Figure 2B), and that had not been previously implicated in autophagy. This finding prompted us to investigate the role of UBA6 in autophagy.

UBA6 depletion increases the levels of LC3B-I without reducing the levels of LC3B-II

UBA6 (ubiquitin-like modifier activating enzyme 6) encodes an E1 Ub-activating enzyme having a cysteine residue that forms a thioester bond with the C-terminal glycine of Ub [47]. To investigate the involvement of UBA6 in autophagy, we initially used siRNAs to knock down (KD) UBA6 in H4 and HeLa cervical carcinoma cells, and examined the levels of the cytosolic (LC3B-I) and membrane-bound (LC3B-II) forms of the Atg8 family member LC3B as indicators of autophagy status [6] (Figures 2C, 2D). Interestingly, we observed that UBA6 KD caused 3-4–fold increases in the levels of LC3B-I without altering the levels of LC3B-II (Figure 2C, 2D). CRISPR/Cas9 KO of UBA6 similarly resulted in increased levels of LC3B-I and unchanged levels of LC3B-II, a phenotype that was partially reversed by transfection with plasmids encoding UBA6 tagged at either the N- or C-terminus with the MYC epitope (Figure 2E, 2F). UBA6 KO caused a similar increase in the levels of LC3A-I but not of other Atg8-family members such as GABARAP and GABARAPL1 (Figure S2B). UBA6 KO also did not cause noticeable changes in the levels of other components of the autophagy machinery, including components of the LC3-conjugation system (ATG3, ATG5, ATG7, ATG12, ATG16), WIPI2, the PI3K complex (BECN1, p-BECN1 and ATG14), the ULK1 complex (ATG13, p-ATG13, ULK1, p-ULK1), and the mTOR signaling pathway (S6K, p-S6K, 4EBP, p-4EBP, TSC2, p-TSC2, AKT, p-AKT) [1] (Figure S2C). Likewise, immunostaining with antibodies to the autophagy machinery components SQSTM1, WIPI2 and ATG9A (Figures S2D-S2F), and to markers for the ER (calnexin), Golgi complex (GM130), early endosomes (RAB5, APPL1, EEA1), lysosomes (LAMP1, LAMTOR4) and the cytoskeleton (β-tubulin, actin) (Figures S2G-S2M), showed no differences in UBA6-KO cells relative to the parental H4 cells. In addition, UBA6-KO cells proliferated at the same rate as WT cells, with doubling times of ~27 h (Figure S3A). Bafilomycin A_1 treatment also caused a similar accumulation of LC3B-II in UBA6-KO and WT cells (Figures 2G, 2H), indicating that autophagy initiation and LC3B conjugation operated normally in UBA6-KO cells. Finally, WT and UBA6-KO cells expressing GFP-mCherry-LC3B and loaded with internalized Alexa Fluor 647-conjugated dextran exhibited similar numbers of autophagosomes (*i.e.*, puncta positive for GFP and mCherry, but negative for Alexa Fluor 647)

and autolysosomes (*i.e.*, puncta positive for mCherry and Alexa Fluor 647, but negative for GFP) (Figures 2I, 2J), indicating that UBA6 KO had no effect on autophagosome-lysosome fusion and lysosome acidification. From all of these experiments we concluded that UBA6 depletion increased LC3B-I levels without affecting its conversion to LC3B-II or its eventual degradation in lysosomes.

UBA6 mediates ubiquitination and proteasomal degradation of LC3B

Since UBA6 is an E1 enzyme [47], we hypothesized that it could decrease LC3-I levels by mediating LC3B-I ubiquitination and proteasomal degradation. Indeed, treatment with the proteasome inhibitor MG132 resulted in a ~3-fold increase in the level of LC3B-I in WT H4 cells, but did not change the already elevated level of LC3B-I in UBA6-KO cells (Figures 3A, 3B). In addition, an in vivo ubiquitination assay showed that transgenic FLAG-tagged LC3B became conjugated with a single copy of HA-tagged Ub (Figure 3C); the level of monoubiquitinated FLAG-LC3B was increased by treatment with MG132 (Figure 3C) and decreased by KO of UBA6 (Figure 3D). Mutation of LC3B-I glycine-120 to alanine – the LC3B-I residue that is conjugated to phosphatidylethanolamine to produce LC3B-II [6] – prevented the association of LC3B with autophagosomes (Figure 3E) without inhibiting ubiquitination (Figure 3F), indicating that LC3B is ubiquitinated in the cytosol. The *in vivo* ubiquitination assay was additionally used to show that FLAG-tagged LC3A and LC3C were also monoubiquitinated, but GABARAP, GABARAPL1 and GABARAPL2 were not (Figure 3G). Finally, we found that endogenous LC3B was also modified with a single HA-Ub moiety (Figure 3H). Taken together, these experiments indicated that UBA6 promotes ubiquitination of cytosolic LC3B-I, targeting it for degradation by the proteasome.

To identify the ubiquitination site on LC3B, we mutated each of its 10 lysines (Figure 4A) to arginine, a residue that cannot be conjugated to Ub. We observed that double K49R-K51R and single K51R mutants were not ubiquitinated, indicating that lysine-51 was the main

ubiquitination site on LC3B (Figures 4B, 4C). Inspection of the structure of LC3B showed that lysine-51 is part of a hydrophobic pocket involved in the recognition of the LC3-interaction region (LIR) of the autophagy receptor SQSTM1 (Figure 4D) [48]. Indeed, co-immunoprecipitation analyses showed that the K51R substitution abolished the interaction of FLAG-LC3B with endogenous forms of SQSTM1 and another autophagy receptor, NBR1 (Figure 4E). These results thus confirmed the critical function of lysine-51 in the recognition of autophagy receptors, and suggested that an additional function of LC3B ubiquitination by UBA6 may be to inhibit this recognition.

BIRC6 acts like UBA6 to decrease the levels of LC3B-I

E1 enzymes function together with E2 Ub-conjugating enzymes and E3 Ub-ligases to add Ub to substrates [49]. To identify the E2 and E3 responsible for LC3B ubiquitination, we conducted another CRISPR/Cas9 KO screen using a lentiviral library of 10,108 sgRNAs targeting all major E1, E2, E3 and deubiquitinating enzymes, as well as other ubiquitination-related proteins (Table S6). As done before, H4-tfLC3B cells were infected with this library, and cells with high GFP:mCherry ratios were enriched by three rounds of FACS (Figures 5A, S3B). Next-generation sequencing and MAGeCK analysis revealed that KO of BIRC6 [Baculoviral IAP (inhibitor of apoptosis) Repeat Containing 6] inhibited quenching of GFP even more potently than UBA6 KO (Figure 5B, Tables S7, S8). The BIRC6 product (also known as BRUCE and APOLLON) is a giant, 528-kDa protein containing an N-terminal BIR (Baculoviral IAP Repeat) domain and a C-terminal UBC (Ub Conjugation) domain [50] (Figure S4A). Previous work showed that BIRC6 combines, in a single polypeptide, E2 and E3 activities towards substrates such as SMAC (second mitochondria-derived activator of caspases) (SMAC) and caspase 9, which are involved in the regulation of apoptosis [50] [51]. In addition, BIRC6 was shown to promote the progression of prostate, liver and colorectal cancers [52] [53] [54] [55].

In further experiments, we found that depletion of BIRC6 by KD or KO in H4 cells increased LC3B-I levels even more dramatically than depletion of UBA6, in both cases with little or no change in the levels of LC3-II (Figures 5C-5E). BIRC6-KO cells also exhibited similar growth rates as WT cells under normal culture conditions (Figure S3A). Incubation with bafilomycin A_1 caused a similar accumulation of LC3B-II in WT, UBA6-KO and BIRC6-KO cells (Figures S3C, S3D). Likewise, the ratio of autophagosomes to autolysosomes determined by fluorescence microscopy as described above was unchanged in BIRC6-KO relative to WT cells (Figures 5F, 5G). These results indicated that BIRC6 depletion increased the levels of LC3-I without inhibiting the conversion of LC3B-I to LC3B-II, nor the degradation of LC3B-II.

To examine the effect of BIRC6 or UBA6 depletion on the activation of autophagy upon nutrient deprivation, WT, BIRC6-KO and UBA6-KO cells were incubated in serum- and amino-acid-free medium for 0.5, 1 and 2 h, after which the cells were analyzed by immunoblotting for LC3B (Figures 5H, 5I, S3C, S3D). We observed that in WT cells the level of LC3B-II increased over the first 30 min and then declined for up to 2 h (Figure 5H, 5I), reflecting the activation and degradation phases of autophagy. In BIRC6-KO or UBA6-KO cells, however, the levels of LC3B-II remained high after 1 and 2 h of starvation (Figures 5H, 5I, S3C, S3D). This effect was likely due to continued replenishment of LC3B-II from the larger pool of LC3B-I in the KO cells. These experiments thus demonstrated that BIRC6 and UBA6 similarly function to reduce LC3B-I levels, limiting the production of LC3B-II during starvation.

BIRC6 cooperates with UBA6 to ubiquitinate LC3B

To examine whether BIRC6, like UBA6, was involved in LC3B ubiquitination, we performed the same *in vivo* assay described above in WT, UBA6-KO and BIRC6-KO cells (Figure 6A). We observed that BIRC6 KO reduced LC3B ubiquitination to an even greater extent than UBA6 KO (Figure 6A). Moreover, we found that FLAG-BIRC6 expressed by transfection in HEK293T cells was able to pull down both endogenous UBA6 (Figure 6B) and transgenic GFP-LC3B (Figure

6C), consistent with both UBA6 and BIRC6 interacting to ubiquitinate LC3B. Additional pulldown analyses using truncated FLAG-BIRC6 constructs showed that the regions spanning amino acids 2201-2800, 3301-3800 and 3801-4300 of BIRC6 interacted with GFP-LC3B (Figures S4A, S4B). The functional cooperation of UBA6 with BIRC6 was directly tested using an *in vitro* ubiquitination assay with different combinations of FLAG-BIRC6 immunopurified from transfected HEK293T cells, recombinant HA-Ub, 6xHis-LC3B and GST-UBA6, and a source of ATP (Figure 6D). Immunoblot analysis of the complete reaction mixture showed a band corresponding to monoubiquitinated LC3B, which was detected by antibodies to both the HA epitope and LC3B (Figure 6D). Omission of any components from the mix abolished this ubiquitination (Figure 6D). In addition, substitution of alanine for cysteine-4597 in the active site of the UBC domain of BIRC6 [50] [51] also abrogated LC3B monoubiquitination (Figure 6E). From these results we concluded that UBA6 and BIRC6 function as E1 and E2/E3 enzymes, respectively, for monoubiquitination of LC3B.

BIRC6 regulates the accumulation of intracellular aggregates

A critical function of autophagy is the degradation of mutant or otherwise damaged proteins [56]. Protein aggregates become ubiquitinated, after which they are recognized by autophagy receptors such as SQSTM1 and NBR1 [57] [58]. These receptors link the aggregates to LC3 on forming autophagosomes, and the aggregates, receptors and LC3 are all eventually degraded in autolysosomes. To examine the impact of BIRC6 KO on this process, we performed cycloheximide (CHX) chase analysis of the degradation of SQSTM1, NBR1 and LC3B in WT and BIRC6-KO cells (Figure 7A). We observed time-dependent disappearance of LC3B-I in both cell lines, although, as expected, BIRC6-KO cells contained higher levels of LC3B-I at all times after the addition of CHX (Figure 7A). Importantly, SQSTM1 and NBR1 exhibited faster rates of degradation in BIRC6-KO relative to WT cells (Figure 7A-C). These observations indicated that

the larger pool of LC3B-I in BIRC6-KO cells promoted faster degradation of autophagy receptors under conditions of protein synthesis inhibition.

We also examined the effect of BIRC6 KO on the clearance of puromycin-induced ALIS (aggresome-like induced structures), which form by aggregation of prematurely terminated translation products and are degraded by autophagy [59] [60]. We observed that addition of puromycin resulted in the emergence of SQSTM1- and Ub-positive ALIS after 2 h in WT cells, and 8 h in BIRC6-KO cells (Figures 7D, 7E). Transfection of BIRC6-KO cells with a plasmid encoding FLAG-BIRC6 restored the accumulation of ALIS at 4 h after puromycin addition (Figure 7F, 7G). Similar observations were made in UBA6 KO cells (Figures S5A, S5B). Additionally, we observed that KD of LC3B rescued the accumulation of ALIS in BIRC6-KO cells treated for 4 h with puromycin (Figure S5C-S5E), consistent with the loss of ALIS in BIRC6-KO cells being due to the elevation of LC3B levels.

Uncontrolled aggregate formation underlies the pathogenesis of many diseases, including various neurodegenerative disorders. Parkinson's disease (PD), in particular, is associated with formation of aberrant α-synuclein aggregates in neurons [61]. To assess a possible effect of BIRC6 depletion on the clearance of α-synuclein aggregates, we transfected rat hippocampal neurons in primary culture with a plasmid encoding the aggregation-prone A53T mutant of α-synuclein [62], with or without a plasmid encoding an shRNA to rat Birc6. In control cells, we observed the formation of numerous aggregates of α-synuclein (Figures 8A-C) that co-localized with endogenous SQSTM1 as well as transgenic HA-Ub and mCherry-LC3B (Figures S6), as previously reported [63] [64]. Transfection with the Birc6 shRNA plasmid, however, resulted in a significant reduction in the number of axonal α-synuclein aggregates (Figure 8A-C). This reduction could be reversed by co-transfection with shRNA-resistant human BIRC6 (Figures S6B, S6C) into the rat Birc6-KD neurons (Figure 8A-C). Moreover, immunoblot analysis showed a decrease in the amount of α-synuclein in Triton-X-100-insoluble fractions in Birc6-KD neurons relative to control and BIRC6-rescue neurons (Figures 8D, 8E),

supporting the conclusion that depletion of Birc6 decreased accumulation of α-synuclein aggregates in rat hippocampal neurons.

Discussion

The results of our study demonstrate that UBA6 and BIRC6 function as E1 and E2/E3 enzymes, respectively, for the monoubiquitination and subsequent proteasomal degradation of the autophagy protein LC3B. This pathway exerts a negative regulatory effect on autophagy, particularly under stress conditions such as nutrient deprivation (Figures 5H, 5I, S3C-D), inhibition of protein synthesis (Figure 7A-C) and formation of protein aggregates (Figures 7D, 7E, 8A-E, S5A-G, S6A-C). Depletion of UBA6 or BIRC6 increases the pool of cytosolic LC3B-I, promoting autophagic flux and clearance of protein aggregates in both non-neuronal and neuronal cells. By dampening LC3 levels, the UBA6-BIRC6 pathway may protect cells from excessive levels of autophagy causing autophagy-dependent cell death [65]. On the other hand, inhibition of UBA6 or BIRC6 could be used to enhance autophagy for the treatment of neurodegenerative disorders caused by abnormal protein aggregation [66].

Comparison to previous CRISPR/Cas9 KO screens

Several recent studies also used genome-wide CRISPR/Cas9 screens to identify novel components and regulators of the autophagy machinery in mammalian cells [67] [68] [69] [70]. As in our study, these screens were performed using cells expressing fluorescently-tagged LC3 or autophagy receptors such as SQSTM1, NPD52, TAX1BP1 or NBR1. All of these screens resulted in the identification of novel candidates, most notably the ER protein TMEM41B, which was shown to participate in autophagosome biogenesis [68] [69] [70]. Our screen differed from previous ones in that we used cells expressing endogenously-tagged LC3B, thus avoiding artifacts of overexpression. Furthermore, we used a more stringent selection procedure involving isolation of cells that were in the top 1% of GFP intensity in the initial screen, and that maintained that level of fluorescent intensity through four additional rounds of sorting and expansion. This stringency likely accounts for the identification of virtually all known

components of the autophagy machinery as top hits in the screen. The relatively high scores of UBA6 and BIRC6 in the whole-genome and ubiquitination screens thus gave us great confidence that these proteins were indeed involved in the regulation of autophagy. It is noteworthy that neither UBA6 nor BIRC6 ranked high in previous screens. This could be due to the overexpression of LC3B from a CMV promoter [70], which likely overwhelmed the ability of UBA6 and BIRC6 to target LC3B for degradation. Indeed, we observed that CMV-driven overexpression of FLAG-tagged LC3B resulted in smaller differences in the levels of this protein in WT, UBA6-KO and BIRC6-KO cells (Figures 3D, 6A). Furthermore, UBA6 and BIRC6 could have been missed in previous screens using autophagy receptors as reporters [67] [68] [70] because the levels of these proteins were unaltered under regular culture conditions, as observed for SQSTM1 and NBR1 in BIRC6-KO cells (Figure 7A). Only when cells were treated with cycloheximide did differences in the turnover of these proteins become apparent (Figure 7A-C).

BIRC6-KO does not affect autophagosome-lysosome fusion in our system

A previous shRNA screen of 710 ubiquitination- and autophagy-related genes identified BIRC6 as an autophagy regulator [71]. In contrast to our findings, however, BIRC6 was reported to promote autophagosome-lysosome fusion through interactions with GABARAP/GABARAPL1 and the SNARE protein syntaxin 17. Moreover, a 1,648-amino-acid N-terminal fragment of BIRC6 was shown to be sufficient for interaction with GABARAP/GABARAPL1 and syntaxin 17, and for association of BIRC6 to lysosomes [71]. In our study, we did not observe any defects in autophagosome-lysosome fusion in BIRC6-KO cells (Figures 5H, 5I), nor did we find localization of BIRC6 to lysosomes but rather to the cytosol (Figure 7F). Moreover, we found that the C-terminally located UBC domain was essential for the role of BIRC6 in LC3B ubiquitination (Figure 6E). We speculate that differences in these studies could be due to the use of different cell types and experimental conditions. In any event, the mechanism involving

LC3B ubiquitination and degradation revealed by our study is consistent with the activity of BIRC6 as an E2/E3 enzyme.

Role of monoubiquitination in LC3B degradation

Our experiments showed that UBA6 and BIRC6 mediate monoubiquitination, rather than polyubiquitination, of LC3B on lysine-51 (Figure 4). The fact that this modification targets LC3B-I for proteasomal degradation is remarkable in light of early notions that monoubiquitination played mainly regulatory, non-degradative roles [72], whereas polyubiquitination was a signal for degradation [73]. More recent evidence, however, suggests that monoubiquitination can also target proteins for proteasomal degradation [74] [75], especially for small proteins of 20-150 residues [76]. Moreover, a systematic analysis revealed that approximately half of all the proteins degraded by proteasomes in human cells are monoubiquitinated or multi-monoubiquitinated [77]. These findings are consistent with our conclusion that monoubiquitination of the 125-amino-acid LC3B is the signal that targets this protein for degradation.

Insights into the role of UBA6 in ubiquitination

UBA6 is one of 8 E1 enzymes involved in the conjugation of 17 Ub-like proteins encoded in the human genome [78]. In particular, UBA6 has been reported to activate both Ub and the Ub-like protein FAT10 [79] [80] [81]. UBA6-mediated FAT10ylation has also been implicated in targeting proteins for proteasomal degradation [82] as well as in the intracellular defense against bacterial infection [83]. Except for one study [84], however, little is known about the role of UBA6-mediated ubiquitination. Herein we show that UBA6 uses BIRC6 as an E2/E3 to ubiquitinate LC3. Nevertheless, small amounts of monoubiquitinated LC3B can still be found in UBA6-KO and BIRC6-KO cells (Figure 6A). This finding suggests that other ubiquitinating enzymes could partially compensate for the absence of UBA6 or BIRC6. These alternative

enzymes, however, likely play minor roles in LC3B ubiquitination, because they were not identified in our screens.

Impact of increased LC3 levels on autophagy and aggregate clearance

Although most of our work dealt with LC3B, LC3A and LC3C were also ubiquitinated (Figure 3G), and UBA6 KO increased LC3A-I in addition to LC3B-I (Figure S2B). In the same assays, GABARAP, GABARAPL1 and GABARAPL2 were not ubiquitinated (Figure 3G) and the levels of GABARAP and GABARAPL1 did not change in UBA6-KO cells (Figure S2B). UBA6-BIRC6–mediated ubiquitination and degradation thus appear to be restricted to the LC3 subgroup of the Atg8 family. Recent studies showed that both LC3 and GABARAP family members contribute to autophagic degradation of protein aggregates and mitochondria [42] [85], although GABARAPs seemed more important [42]. We find that increasing the levels of LC3B by BIRC6-KO in H4 neuroglioma cells reduces the half-life of SQSTM1 and NBR1 (Figure 7A-C). Moreover, depletion of BIRC6 or UBA6 decreases the formation of SQSTM1- and Ub-decorated protein aggregates in both H4 cells (Figures 7F-E, S5) and rat hippocampal neurons (Figure 8A-E, S6). Therefore, at least in these CNS-derived cells, decreasing the levels of LC3 enhances autophagic flux and decreases accumulation of protein aggregates. Our findings are in line with a previous report that overexpression of LC3B in a transgenic mouse model of Alzheimer's disease inhibited amyloid-β-peptide-induced neuron degeneration by enhancing autophagy flux [86]. In addition, another study showed that overexpression of a LC3B transgene attenuated lung injury in a mouse model of sepsis, probably by enhancement of autophagosome clearance [87]. These findings do not only support the notion that elevated LC3 levels promote autophagy flux, but also suggest that increasing LC3 levels could have therapeutic applications.

Potential use of UBA6 or BIRC6 inhibition to treat protein aggregation diseases

Intracellular accumulation of pathogenic protein aggregates is a common cause of various neurodegenerative disorders [66]. This accumulation usually results from overproduction of normal proteins or from synthesis of mutant proteins that overwhelm the capacity of the autophagy machinery to clear them. An example of such disorders is PD, a neurodegenerative disease characterized by the presence of Lewy bodies containing aggregated α-synuclein [61]. Since α-synuclein aggregates are mainly degraded by autophagy [88], autophagy enhancement has been proposed as a possible therapy for PD [89]. Indeed, autophagy enhancing agents targeting AMPK [90], mTORC1 [91] [92], BECN1 [93] and lysosomal glucocerebrosidase [94] have been shown to increase α-synuclein clearance and to have a neuroprotective effect in animal models of PD. However, targeting AMPK and mTORC1 is problematic because, as central nodes of nutrient and energy signaling pathways, they regulate numerous of cellular processes, including cell growth, protein synthesis and metabolism [95] [96]. The decreased accumulation of α-synuclein aggregates by depletion of UBA6 or BIRC6 shown here suggests that these proteins could also be targeted for pharmacologic treatment of PD and other protein aggregation disorders.

Materials and methods

Cell culture and transfection

H4, H4-derived KO, HeLa and HEK293T cells were grown in Dulbecco's modified Eagle's medium (DMEM, Corning, 15-013-CV) with 10 % fetal bovine serum (FBS, Corning, 35-011-CV), 100 IU/ml penicillin, 100 µg/ml streptomycin (Corning, 30-002-CI) and 2 mM L-glutamine (Corning, 25-005-CI) at 37°C, 5 % CO_2. Transfection of siRNAs was performed with Oligofectamine (Thermo Fisher Scientific, 12252011), and transfection of plasmids was performed with Lipofectamine 2000 (Thermo Fisher Scientific, 11668019), both according to the manufacturers' instructions. Starvation was performed by incubating cells with DMEM without amino acids (MyBioSource, MBS653087).

Antibodies and chemicals

We used primary antibodies to the following proteins: LC3B (Cell Signaling Technology, 3868), UBA6 (Cell Signaling Technology, 13386), β-tubulin (Cell Signaling Technology, 2146), MYC epitope (Santa Cruz Biotechnology, sc-789), Ub (for Western blotting, Thermo Fisher Scientific, 13-1600), Ub (for immunofluorescence assay, Enzo Life Sciences, BML-PW8805-0500), HA epitope (BioLegend, 901501), FLAG epitope (Sigma-Aldrich, F1804), SQSTM1 (for Western blotting, BD Biosciences, 610833), SQSTM1 (for immunofluorescence assay, Enzo Life Sciences, BML-PW9860-0100), NBR1 (Cell Signaling Technology, 9891), NIX (Cell Signaling Technology, 12396), BIRC6 (Cell Signaling Technology, 8765), GFP (Thermo Fisher Scientific, A11122), Actin (Cell Signaling Technology, 3700). HRP-conjugated secondary antibodies were from Perkin Elmer (NEF822001EA, NEF812001EA). Secondary antibodies conjugated to Alexa Fluor dyes were from Thermo Fisher Scientific.

Bafilomycin A_1 (B1793), MG132 (M7449), Cycloheximide (C4859), puromycin (P8833) and polybrene (hexadimethrine bromide, H9268) were from Sigma-Aldrich.

The siRNA oligos targeting to UBA6 (4392420-s30516, -s30517), BIRC6 (4427037-s33037, -s33038, -s33039) were from Thermo Fisher Scientific. Non-targeting siRNA (UGGUUUACAUGUCGACUAAUUU) was synthesized from Eurofins Scientific.

Plasmids

Plasmids encoding HA-Ubiquitin (18712) and GFP-α-synuclein A53T (40823) were obtained from Addgene. A FLAG-BRIC6 plasmid was a gift from Dr. Mikihiko Naito (Kawasaki Hospital, Kobe, Japan). Plasmids encoding GFP-LC3B and GFP-mCherry-LC3B were previously described [41]. FLAG-LC3A, FLAG-LC3B, FLAG-LC3C, FLAG-GABARAP, FLAG-GABARAPL1, FLAG-GABARAPL2 were generated by subcloning coding sequences for each protein into pCI-neo vector (Promega, E1841) with N-terminal FLAG tag. FLAG-LC3B-G120A, FLAG-LC3B-K5R-K8R, FLAG-LC3B-K30R, FLAG-LC3B-K39R-K42R, FLAG-LC3B-K49R-K51R, FLAG-LC3B-K65R, FLAG-LC3B-K103R, FLAG-LC3B-K122R, FLAG-LC3B-K49R, FLAG-LC3B-K51R and FLAG-BIRC6-C4597A were generated using Q5® Site-Directed Mutagenesis Kit (New England Biolabs, E0552). The pSuper-Birc6-shRNA plasmid was generated by cloning shRNA for rat Birc6 (5′-CACCCCAGTAGTCATACCA-3′) into pSuper.neo+mCherry [97].

Genome editing by CRISPR/Cas9

To generate cells expressing endogenously tagged GFP-mCherry-LC3B (H4-tfLC3B), the targeting sequence for LC3B (TTCTCCGACGGCATGGTGCA) was cloned into the pSpCas9 (BB)-2A-GFP plasmid (Addgene, 48138). Donor DNA for homology recombination consisted of a 1000-bp left homology arm, DNA sequence encoding GFP-mCherry, and 1000-bp right homology arm (Fig S1A). H4 cells were co-transfected with CRISPR/Cas9 plasmid and donor

DNA. GFP-positive cells were sorted on a FACS Aria II Flow Cytometer (BD Biosciences, San Jose, CA, USA) after 24 h, and propagated. GFP-mCherry double-positive cells were collected by FACS one week after transfection. Single-cell clones were isolated by serial dilution on 96-well plates. The insertion of the GFP-mCherry fragment was confirmed by DNA sequencing and immunoblotting (Figure S1B).

UBA6-KO and BIRC6-KO H4 cells were generated by CRISPR/Cas9 as previously described [40]. The targeting sequences for UBA6 (CGAGCCTGTGGCCGCCCATC and CTCCGGTCGAGAGCGAGTTC) and BIRC6 (GCATGCACTGCGACGCCGAC and TCTCGCTTCCCCGAGTCGCG) were cloned separately into pSpCas9 (BB)-2A-GFP plasmid. H4 cells were co-transfected with two plasmids containing the different targeting sequences for the same gene, and GFP-positive cells were selected on a FACS Aria II Flow Cytometer after 24 h. Single-cell clones were isolated on 96-well plates. After 14 days, genomic DNA was extracted, and the cleavage of the target sequence tested by PCR. The KO was confirmed by DNA sequencing and immunoblotting.

Genome-wide CRISPR/Cas9 screen

A human CRISPR KO Pooled Library (GeCKO v2) (Addgene, 1000000048) was used to introduce mutations in the H4-tfLC3B genome. HEK293T cells were co-transfected with GeCKO v2 library, pMD2.G (Addgene, 12259) and psPAX (Addgene, 12260). The supernatants were collected 48 h after transfection, filtered on a 0.2-μm filter unit, and stored at -80°C. To test the viral titer, 0.5 million H4-tfLC3B cells were seeded on each well of a 6-well plate 24 h prior to infection. The cells were incubated with lentiviral supernatants with 5 μg/ml polybrene for 4 h, and one extra well of cells was incubated with regular medium without viral supernatants as control. Viral supernatants were then discarded, and fresh medium was added. The following day, cells were trypsinized and 10,000 cells were seeded into each well of a 24-well plate in duplicate. The next day, one well was supplemented with 1 μg/ml puromycin, while the other

well was maintained in regular medium. When puromycin killed all the cells in the no-virus condition, the number of cells in each well was counted. The multiplicity of infection (MOI) was calculated by dividing the number of cells in puromycin-selected wells by that in the unselected wells.

For the large-scale screen, 200 million H4-tfLC3B cells were infected with the lentiviral pool at a MOI of 0.3. The transduced cells were selected by adding 1 μg/ml puromycin 24 h after infection. After puromycin selection for 7 days, the initial screen was performed by collecting the top 1% cells with increased GFP signal by sorting on a FACS Aria II Flow Cytometer. The sorted cells were propagated to 10 million and subjected to the next round of sorting with the same gating.

Next-generation sequencing

Genomic DNA from 60 million unsorted cells (500× coverage of the GeCKO v2 library) and 6 million sorted cells was isolated using Blood & Cell Culture DNA Midi Kit (QIAGEN, 13343) according to the manufacturer's instructions. DNA fragments encoding sgRNAs were amplified by PCR from 250 μg (for unsorted cells) or 25 μg (for sorted cells) genomic DNA using the primers: AATGGACTATCATATGCTTACCGTAACTTGAAAGTATTTCG / CAAAAAAGCACCGACTCGGTGCCACTTTTTCAAG. A second PCR was then performed to attach Illumina overhang adapters using the primer set TCGTCGGCAGCGTCAGATGTGTATAAGAGACAGGCTTACCGTAACTTGAAAGTATTTCG /GTCTCGTGGGCTCGGAGATGTGTATAAGAGACAGACCGACTCGGTGCCACTTTTTCAAG. Indices and Illumina sequencing adapters were added using the Nextera XT Index kit following the manufacturer's protocol (Illumina). Libraries were multiplexed and sequenced on an Illumina MiSeq using v2 chemistry generating an average of 2.5 million reads (2 x 150-bp) per sample. The sgRNA sequences that were 20-bp in length and that completely matched the

GeCKO v2 library were selected, and the number of reads of each sgRNA was calculated and analyzed using the MAGeCK algorithm.

Secondary and ubiquitination screen

The pooled secondary and ubiquitination-related CRISPR library were constructed based on the sgRNA sequences from two published whole genome CRISPR screens [36] [46]. In the secondary library, 432 top-ranked genes from the primary screen were targeted, while in the ubiquitination library, 661 major E1, E2, E3 and deubiquitinating enzymes were targeted. Both libraries contained 1000 nontargeting sgRNAs as control. Oligonucleotides containing the guide sequences were synthesized by Twist Bioscience as a pool, and amplified by PCR using primers Oligo-Fwd: GTAACTTGAAAGTATTTCGATTTCTT GGCTTTATATATCTTGTGGAAAGGAC GAAACACC and Oligo-Knockout-Rev: ACTTTTTCAAGTTGATAACGGACTAG CCTTATTTTAACTTGCTATTTCTAGCT CTAAAAC. PCR products were ligated into lentiCRISPR v2 (Addgene, 52961) using Gibson Assembly® Master Mix (New England Biolabs, E2611). The ligation products were purified and concentrated by isopropanol precipitation, then transformed into Endura ElectroCompetent cells (Lucigen, 60242) according to manufacturer's directions. The number of colonies were counted to ensure there were more than 500 colonies per sgRNA in the library. The colonies were collected and subjected to plasmid preparation.

The production of the lentiviral pool and screens in H4-tfLC3 cells were performed as described in the primary screen.

Flow cytofluorometry

After starvation, bafilomcyin A_1 incubation, or library infection, cells were detached with 0.5% trypsin and 5 mM EDTA, pelleted and resuspended in regular DMEM with 10% FBS. Fluorescence intensities were measured on an LSRFortessa™ Flow Cytometer (BD Biosciences),

while the cells with increased GFP signal were collected on an FACS Aria II Flow Cytometer. The scatter plots were generated with FlowJo.

Immunofluorescence microscopy and live-cell imaging

Cells were grown on glass coverslips coated with 5 μg/ml fibronectin (Sigma-Aldrich, F2006) for 24 h prior to the experiment. Cells were washed once with PBS, fixed in 4 % paraformaldehyde (PFA) in PBS for 20 min, and permeabilized in 0.2 % Triton X-100 (Sigma-Aldrich, T9284) for 20 min. Cells were incubated with primary antibodies diluted in 0.2 % BSA (Sigma-Aldrich, A7030) in PBS for 1 h at 37°C, washed three times with PBS, and incubated with Alexa Fluor-conjugated secondary antibodies (Thermo Fisher Scientific) for 30 min at 37°C. Cells were washed with PBS and mounted with DAPI-Fluoromount-G (Electron Microscopy Sciences, 17984-24).

Neurons were washed once with PBS-CM (PBS supplemented with 0.1 mM $CaCl_2$ and 1 mM $MgCl_2$), fixed with 4% PFA and 4% sucrose in PBS-CM, and permeabilized with 0.2% Triton X-100 in PBS-CM. Neurons were blocked with 0.2% gelatin in PBS-CM and incubated with primary antibodies diluted in 0.2% gelatin for 1 h at 37°C, then washed three times with PBS-CM and incubated with secondary antibodies. After three more washes with PBS-CM and one wash with water, neurons were mounted with DAPI-Fluoromount-G.

Live-cell imaging was performed in four-well Nunc Lab-Tek Chambered Coverglasses (Thermo Fisher Scientific, 155383) coated with 5 μg/ml fibronectin. To inhibit lysosomal degradation, cells were incubated with 50 ng/ml bafilomycin A_1 for 2 h prior to imaging. Labeling of lysosomes was performed by loading cells with Alexa Fluor 647-dextran for 16 h after transfection. Fluorescence was visualized on a Zeiss LSM780 confocal microscope (Carl Zeiss). Image analysis was performed with ImageJ.

Immunoprecipitation and immunoblotting

H4 cells were grown to ~90% confluency, washed with PBS, harvested by scraping, and lysed on ice for 20 min in lysis buffer (150 mM NaCl, 50 mM Tris-HCl [pH 7.4], 5 mM EDTA, 1% Triton X-100, 3% glycerol [Sigma-Aldrich, G6279]) with a protease inhibitor cocktail (Roche, 11697498001). Cytosolic extracts were cleared by centrifugation at 13,000 g for 20 min at 4°C and incubated with anti-FLAG (Sigma-Aldrich, F4799) or anti-HA (Thermo Fisher Scientific, 88836) magnetic beads at 4°C for 4 h. After washing three times in lysis buffer, proteins were eluted from beads by incubation with 3xFLAG peptide (Thermo Fisher Scientific, A36798) or HA peptide (Thermo Fisher Scientific, 26184).

***In vitro* ubiquitination assay**

For the *in vitro* ubiquitination assay, FLAG-tagged BIRC6 was immunoisolated as described [50]. Briefly, HEK293T cells expressing FLAG-tagged BIRC6 were lysed on ice for 20 min in digitonin lysis buffer (20 mM HEPES pH 7.5, 10 mM KCl, 1.5 mM $MgCl_2$, 1 mM EDTA, 0.05% digitonin [Sigma-Aldrich, D141], 250 mM sucrose) with a protease inhibitor cocktail. Cell lysates were cleared by centrifugation at 20,000 g for 15 min at 4°C, and NaCl was added to 150 mM final concentration. Cleared lysates were incubated with anti-FLAG magnetic beads at 4°C for 4 h. Beads were washed with 1% Triton X-100 in PBS followed by 0.1% Triton X-100 in PBS, and PBS.

Immunopurified FLAG-BIRC6 on beads was incubated with the reaction mixture containing 125 nM GST-UBA6 (Boston Biochem, E-307), 6 μM 6xHis-LC3B (ProSpec Bio, PRO-076), 10 μM HA-Ub (Boston Biochem, U-110), and 10 μM MgATP (Boston Biochem, B-20), in a final volume of 30 μl of E3 ligase buffer (Boston Biochem, B-71) at 37°C for 1 h. Reactions were terminated by mixing supernatants with 4xLDS (lithium dodecyl sulfate) sample buffer (Thermo Fisher Scientific, NP0007). FLAG-BIRC6 was eluted from the beads by incubation with 3xFLAG peptide. Samples were analyzed by immunoblotting.

Preparation, culture and transfection of neurons

Briefly, primary rat hippocampal neurons were prepared from Sprague-Dawley rats at embryonic stage E18 as previously described [98]. Hipocampi were dissociated with 0.25% trypsin in 2.2 mM EDTA and plated onto polylysine-coated plates. Neurons were maintained in DMEM supplemented with 10% horse serum for 3 h, then medium was changed to Neurobasal medium (Thermo Fisher Scientific, 21103049), supplemented with B27 serum-free (Thermo Fisher Scientific, A3582801), 100 U/ml penicillin and 100 µg/ml streptomycin. Neurons were transfected with the indicated plasmids using lipofectamine 2000 at day-in-vitro 3 (DIV3) and analyzed at DIV7 by immunofluorescence microscopy or subcellular fractionation.

Extraction of soluble and insoluble α-synuclein

Cultured primary hippocampal neurons were lysed on ice for 15 min in Triton buffer (50 mM Tris-HCl pH 7.5, 150 mM NaCl, 1% Triton X-100, and 1 mM EDTA supplemented with protease inhibitor cocktail) and centrifuged at 15,000 g for 10 min at 4°C. The supernatant was collected as the Triton-soluble fraction. After washing three times with Triton buffer, the pellet was resuspended in SDS buffer (Triton buffer supplemented with 5% SDS [Sigma-Aldrich, L3771]), heated at 95°C for 10 min, and then centrifuged at 15,000 g for 10 min at room temperature. The supernatant was collected as the Triton-insoluble fraction. Triton-soluble and -insoluble fractions were mixed with LDS sample buffer and analyzed by immunoblotting.

Quantification and statistical analyses

All graphs represent data were from at least three independent experiments. As indicated in the legends, statistical comparisons were made using either one-way analysis of variance (ANOVA) with Dunnett's multiple comparisons test, two-way ANOVA with Tukey's multiple

comparisons test, or Student's *t* test as indicated by the Prism 7 software. Numerical *p*-values are indicated in each graph; n.s. stands for not-significant differences.

Author contributions

R.J. and J.S.B. conceived the project. R.J. performed all the experiments. R.J. and J.S.B. analyzed the data and wrote the manuscript.

Declaration of interests

The authors declare no competing interests.

Acknowledgments

We thank Mikihiko Naito for kind gift of FLAG-BIRC6 plasmid, Steven Coon and other members of the Molecular Genomics Core of NICHD for next-generation sequencing, Xiaolin Zhu for excellent technical assistance, and other members of the Bonifacino lab for helpful discussions. This work was funded by the Intramural Program of NICHD (ZIA HD001607).

References

1. Bento CF, Renna M, Ghislat G et al. Mammalian Autophagy: How Does It Work. Annu Rev Biochem. 2016;85:685-713.
2. Dikic I, Elazar Z. Mechanism and medical implications of mammalian autophagy. Nat Rev Mol Cell Biol. 2018;19:349-364.
3. Levine B, Kroemer G. Autophagy in the pathogenesis of disease. Cell. 2008;132:27-42.
4. Birgisdottir ÅB, Lamark T, Johansen T. The LIR motif - crucial for selective autophagy. J Cell Sci. 2013;126:3237-3247.
5. Wild P, McEwan DG, Dikic I. The LC3 interactome at a glance. J Cell Sci. 2014;127:3-9.
6. Kabeya Y, Mizushima N, Yamamoto A, Oshitani-Okamoto S, Ohsumi Y, Yoshimori T. LC3, GABARAP and GATE16 localize to autophagosomal membrane depending on form-II formation. J Cell Sci. 2004;117:2805-2812.
7. Khaminets A, Heinrich T, Mari M et al. Regulation of endoplasmic reticulum turnover by selective autophagy. Nature. 2015;522:354-358.
8. Fumagalli F, Noack J, Bergmann TJ et al. Translocon component Sec62 acts in endoplasmic reticulum turnover during stress recovery. Nat Cell Biol. 2016;18:1173-1184.
9. Grumati P, Morozzi G, Hölper S et al. Full length RTN3 regulates turnover of tubular endoplasmic reticulum via selective autophagy. Elife. 2017;6:pii: e25555. doi: 10.7554/eLife.25555.
10. Smith MD, Harley ME, Kemp AJ et al. CCPG1 Is a Non-canonical Autophagy Cargo Receptor Essential for ER-Phagy and Pancreatic ER Proteostasis. Dev Cell. 2018;44:217-232.e11.
11. Chino H, Hatta T, Natsume T, Mizushima N. Intrinsically Disordered Protein TEX264 Mediates ER-phagy. Mol Cell. 2019;74:909-921.e6.

12. An H, Ordureau A, Paulo JA, Shoemaker CJ, Denic V, Harper JW. TEX264 Is an Endoplasmic Reticulum-Resident ATG8-Interacting Protein Critical for ER Remodeling during Nutrient Stress. Mol Cell. 2019;74:891-908.e10.
13. Tanida I, Minematsu-Ikeguchi N, Ueno T, Kominami E. Lysosomal turnover, but not a cellular level, of endogenous LC3 is a marker for autophagy. Autophagy. 2005;1:84-91.
14. Bjørkøy G, Lamark T, Brech A et al. p62/SQSTM1 forms protein aggregates degraded by autophagy and has a protective effect on huntingtin-induced cell death. J Cell Biol. 2005;171:603-614.
15. Egan DF, Chun MG, Vamos M et al. Small Molecule Inhibition of the Autophagy Kinase ULK1 and Identification of ULK1 Substrates. Mol Cell. 2015;59:285-297.
16. Russell RC, Tian Y, Yuan H et al. ULK1 induces autophagy by phosphorylating Beclin-1 and activating VPS34 lipid kinase. Nat Cell Biol. 2013;15:741-750.
17. Park JM, Jung CH, Seo M et al. The ULK1 complex mediates MTORC1 signaling to the autophagy initiation machinery via binding and phosphorylating ATG14. Autophagy. 2016;12:547-564.
18. Egan DF, Shackelford DB, Mihaylova MM et al. Phosphorylation of ULK1 (hATG1) by AMP-activated protein kinase connects energy sensing to mitophagy. Science. 2011;331:456-461.
19. Kim J, Kundu M, Viollet B, Guan KL. AMPK and mTOR regulate autophagy through direct phosphorylation of Ulk1. Nat Cell Biol. 2011;13:132-141.
20. Kim YM, Jung CH, Seo M et al. mTORC1 phosphorylates UVRAG to negatively regulate autophagosome and endosome maturation. Mol Cell. 2015;57:207-218.
21. Shi CS, Kehrl JH. TRAF6 and A20 regulate lysine 63-linked ubiquitination of Beclin-1 to control TLR4-induced autophagy. Sci Signal. 2010;3:ra42.
22. Nazio F, Strappazzon F, Antonioli M et al. mTOR inhibits autophagy by controlling ULK1 ubiquitylation, self-association and function through AMBRA1 and TRAF6. Nat Cell Biol. 2013;15:406-416.

23. Liu Z, Chen P, Gao H et al. Ubiquitylation of autophagy receptor Optineurin by HACE1 activates selective autophagy for tumor suppression. Cancer Cell. 2014;26:106-120.
24. Linares JF, Duran A, Yajima T, Pasparakis M, Moscat J, Diaz-Meco MT. K63 polyubiquitination and activation of mTOR by the p62-TRAF6 complex in nutrient-activated cells. Mol Cell. 2013;51:283-296.
25. Liu CC, Lin YC, Chen YH et al. Cul3-KLHL20 Ubiquitin Ligase Governs the Turnover of ULK1 and VPS34 Complexes to Control Autophagy Termination. Mol Cell. 2016;61:84-97.
26. Platta HW, Abrahamsen H, Thoresen SB, Stenmark H. Nedd4-dependent lysine-11-linked polyubiquitination of the tumour suppressor Beclin 1. Biochem J. 2012;441:399-406.
27. Xu C, Feng K, Zhao X et al. Regulation of autophagy by E3 ubiquitin ligase RNF216 through BECN1 ubiquitination. Autophagy. 2014;10:2239-2250.
28. Noda T, Ohsumi Y. Tor, a phosphatidylinositol kinase homologue, controls autophagy in yeast. J Biol Chem. 1998;273:3963-3966.
29. Thoreen CC, Kang SA, Chang JW et al. An ATP-competitive mammalian target of rapamycin inhibitor reveals rapamycin-resistant functions of mTORC1. J Biol Chem. 2009;284:8023-8032.
30. Shi WY, Xiao D, Wang L et al. Therapeutic metformin/AMPK activation blocked lymphoma cell growth via inhibition of mTOR pathway and induction of autophagy. Cell Death Dis. 2012;3:e275.
31. Blommaart EF, Krause U, Schellens JP, Vreeling-Sindelárová H, Meijer AJ. The phosphatidylinositol 3-kinase inhibitors wortmannin and LY294002 inhibit autophagy in isolated rat hepatocytes. Eur J Biochem. 1997;243:240-246.
32. Wu YT, Tan HL, Shui G et al. Dual role of 3-methyladenine in modulation of autophagy via different temporal patterns of inhibition on class I and III phosphoinositide 3-kinase. J Biol Chem. 2010;285:10850-10861.
33. Liu J, Xia H, Kim M et al. Beclin1 controls the levels of p53 by regulating the deubiquitination activity of USP10 and USP13. Cell. 2011;147:223-234.

34. Jiang X, Overholtzer M, Thompson CB. Autophagy in cellular metabolism and cancer. J Clin Invest. 2015;125:47-54.
35. Kimura S, Noda T, Yoshimori T. Dissection of the autophagosome maturation process by a novel reporter protein, tandem fluorescent-tagged LC3. Autophagy. 2007;3:452-460.
36. Joung J, Konermann S, Gootenberg JS et al. Genome-scale CRISPR-Cas9 knockout and transcriptional activation screening. Nat Protoc. 2017;12:828-863.
37. Kuma A, Hatano M, Matsui M et al. The role of autophagy during the early neonatal starvation period. Nature. 2004;432:1032-1036.
38. Sanjana NE, Shalem O, Zhang F. Improved vectors and genome-wide libraries for CRISPR screening.[letter]. Nat Methods 2014;11(8):783-784.
39. Li W, Xu H, Xiao T et al. MAGeCK enables robust identification of essential genes from genome-scale CRISPR/Cas9 knockout screens. Genome Biol. 2014;15:554.
40. Pu J, Schindler C, Jia R, Jarnik M, Backlund P, Bonifacino JS. BORC, a multisubunit complex that regulates lysosome positioning. Dev Cell. 2015;33:176-188.
41. Jia R, Guardia CM, Pu J, Chen Y, Bonifacino JS. BORC coordinates encounter and fusion of lysosomes with autophagosomes. Autophagy. 2017;13:1648-1663.
42. Vaites LP, Paulo JA, Huttlin EL, Harper JW. Systematic Analysis of Human Cells Lacking ATG8 Proteins Uncovers Roles for GABARAPs and the CCZ1/MON1 Regulator C18orf8/RMC1 in Macroautophagic and Selective Autophagic Flux. Mol Cell Biol. 2018;38:pii: e00392-17. doi: 10.1128/MCB.00392.
43. Liang XH, Jackson S, Seaman M et al. Induction of autophagy and inhibition of tumorigenesis by beclin 1. Nature. 1999;402:672-676.
44. Webster CP, Smith EF, Bauer CS et al. The C9orf72 protein interacts with Rab1a and the ULK1 complex to regulate initiation of autophagy. EMBO J. 2016;35:1656-1676.
45. Wang Z, Miao G, Xue X et al. The Vici Syndrome Protein EPG5 Is a Rab7 Effector that Determines the Fusion Specificity of Autophagosomes with Late Endosomes/Lysosomes. Mol Cell. 2016;63:781-795.

46. Wang T, Birsoy K, Hughes NW et al. Identification and characterization of essential genes in the human genome. Science. 2015;350:1096-1101.
47. Groettrup M, Pelzer C, Schmidtke G, Hofmann K. Activating the ubiquitin family: UBA6 challenges the field. Trends Biochem Sci. 2008;33:230-237.
48. Ichimura Y, Kumanomidou T, Sou YS et al. Structural basis for sorting mechanism of p62 in selective autophagy. J Biol Chem. 2008;283:22847-22857.
49. Pickart CM. Mechanisms underlying ubiquitination. Annu Rev Biochem. 2001;70:503-533.
50. Bartke T, Pohl C, Pyrowolakis G, Jentsch S. Dual role of BRUCE as an antiapoptotic IAP and a chimeric E2/E3 ubiquitin ligase. Mol Cell. 2004;14:801-811.
51. Hao Y, Sekine K, Kawabata A et al. Apollon ubiquitinates SMAC and caspase-9, and has an essential cytoprotection function. Nat Cell Biol. 2004;6:849-860.
52. Low CG, Luk IS, Lin D et al. BIRC6 protein, an inhibitor of apoptosis: role in survival of human prostate cancer cells. PLoS One. 2013;8:e55837.
53. Ren J, Shi M, Liu R et al. The Birc6 (Bruce) gene regulates p53 and the mitochondrial pathway of apoptosis and is essential for mouse embryonic development. Proc Natl Acad Sci U S A. 2005;102:565-570.
54. Hu T, Weng S, Tang W et al. Overexpression of BIRC6 Is a Predictor of Prognosis for Colorectal Cancer. PLoS One. 2015;10:e0125281.
55. Tang W, Xue R, Weng S et al. BIRC6 promotes hepatocellular carcinogenesis: interaction of BIRC6 with p53 facilitating p53 degradation. Int J Cancer. 2015;136:E475-87.
56. Lim J, Yue Z. Neuronal aggregates: formation, clearance, and spreading. Dev Cell. 2015;32:491-501.
57. Pankiv S, Clausen TH, Lamark T et al. p62/SQSTM1 binds directly to Atg8/LC3 to facilitate degradation of ubiquitinated protein aggregates by autophagy. J Biol Chem. 2007;282:24131-24145.
58. Kirkin V, Lamark T, Johansen T, Dikic I. NBR1 cooperates with p62 in selective autophagy of ubiquitinated targets. Autophagy. 2009;5:732-733.

59. McEwan DG, Popovic D, Gubas A et al. PLEKHM1 regulates autophagosome-lysosome fusion through HOPS complex and LC3/GABARAP proteins. Mol Cell. 2015;57:39-54.
60. Szeto J, Kaniuk NA, Canadien V et al. ALIS are stress-induced protein storage compartments for substrates of the proteasome and autophagy. Autophagy. 2006;2:189-199.
61. Polymeropoulos MH, Lavedan C, Leroy E et al. Mutation in the alpha-synuclein gene identified in families with Parkinson's disease. Science. 1997;276:2045-2047.
62. Conway KA, Harper JD, Lansbury PT. Accelerated in vitro fibril formation by a mutant alpha-synuclein linked to early-onset Parkinson disease. Nat Med. 1998;4:1318-1320.
63. Watanabe Y, Tatebe H, Taguchi K et al. p62/SQSTM1-dependent autophagy of Lewy body-like α-synuclein inclusions. PLoS One. 2012;7:e52868.
64. Alexopoulou Z, Lang J, Perrett RM et al. Deubiquitinase Usp8 regulates α-synuclein clearance and modifies its toxicity in Lewy body disease. Proc Natl Acad Sci U S A. 2016;113:E4688-4697.
65. Liu Y, Levine B. Autosis and autophagic cell death: the dark side of autophagy. Cell Death Differ. 2015;22:367-376.
66. Ross CA, Poirier MA. Protein aggregation and neurodegenerative disease. Nat Med. 2004;10 Suppl:S10-7.
67. DeJesus R, Moretti F, McAllister G et al. Functional CRISPR screening identifies the ufmylation pathway as a regulator of SQSTM1/p62. Elife. 2016;5: pii: e17290. doi: 10.7554/eLife.17290.
68. Moretti F, Bergman P, Dodgson S et al. TMEM41B is a novel regulator of autophagy and lipid mobilization. EMBO Rep. 2018;19:pii: e45889. doi: 10.15252/embr.201845889.
69. Morita K, Hama Y, Izume T et al. Genome-wide CRISPR screen identifies TMEM41B as a gene required for autophagosome formation. J Cell Biol. 2018;217:3817-3828.

70. Shoemaker CJ, Huang TQ, Weir NR, Polyakov NJ, Schultz SW, Denic V. CRISPR screening using an expanded toolkit of autophagy reporters identifies TMEM41B as a novel autophagy factor. PLoS Biol. 2019;17:e2007044.
71. Ebner P, Poetsch I, Deszcz L, Hoffmann T, Zuber J, Ikeda F. The IAP family member BRUCE regulates autophagosome-lysosome fusion. Nat Commun. 2018;9:599.
72. Haglund K, Di Fiore PP, Dikic I. Distinct monoubiquitin signals in receptor endocytosis. Trends Biochem Sci. 2003;28:598-603.
73. Thrower JS, Hoffman L, Rechsteiner M, Pickart CM. Recognition of the polyubiquitin proteolytic signal. EMBO J. 2000;19:94-102.
74. Boutet SC, Disatnik MH, Chan LS, Iori K, Rando TA. Regulation of Pax3 by proteasomal degradation of monoubiquitinated protein in skeletal muscle progenitors. Cell. 2007;130:349-362.
75. Dimova NV, Hathaway NA, Lee BH et al. APC/C-mediated multiple monoubiquitylation provides an alternative degradation signal for cyclin B1. Nat Cell Biol. 2012;14:168-176.
76. Shabek N, Herman-Bachinsky Y, Buchsbaum S et al. The size of the proteasomal substrate determines whether its degradation will be mediated by mono- or polyubiquitylation. Mol Cell. 2012;48:87-97.
77. Braten O, Livneh I, Ziv T et al. Numerous proteins with unique characteristics are degraded by the 26S proteasome following monoubiquitination. Proc Natl Acad Sci U S A. 2016;113:E4639-4647.
78. Schulman BA, Harper JW. Ubiquitin-like protein activation by E1 enzymes: the apex for downstream signalling pathways. Nat Rev Mol Cell Biol. 2009;10:319-331.
79. Pelzer C, Kassner I, Matentzoglu K et al. UBE1L2, a novel E1 enzyme specific for ubiquitin. J Biol Chem. 2007;282:23010-23014.
80. Chiu YH, Sun Q, Chen ZJ. E1-L2 activates both ubiquitin and FAT10. Mol Cell. 2007;27:1014-1023.

81. Jin J, Li X, Gygi SP, Harper JW. Dual E1 activation systems for ubiquitin differentially regulate E2 enzyme charging. Nature. 2007;447:1135-1138.
82. Aichem A, Kalveram B, Spinnenhirn V et al. The proteomic analysis of endogenous FAT10 substrates identifies p62/SQSTM1 as a substrate of FAT10ylation. J Cell Sci. 2012;125:4576-4585.
83. Spinnenhirn V, Farhan H, Basler M, Aichem A, Canaan A, Groettrup M. The ubiquitin-like modifier FAT10 decorates autophagy-targeted Salmonella and contributes to Salmonella resistance in mice. J Cell Sci. 2014;127:4883-4893.
84. Lee PC, Sowa ME, Gygi SP, Harper JW. Alternative ubiquitin activation/conjugation cascades interact with N-end rule ubiquitin ligases to control degradation of RGS proteins. Mol Cell. 2011;43:392-405.
85. Nguyen TN, Padman BS, Usher J, Oorschot V, Ramm G, Lazarou M. Atg8 family LC3/GABARAP proteins are crucial for autophagosome-lysosome fusion but not autophagosome formation during PINK1/Parkin mitophagy and starvation. J Cell Biol. 2016;215:857-874.
86. Hung SY, Huang WP, Liou HC, Fu WM. LC3 overexpression reduces Aβ neurotoxicity through increasing α7nAchR expression and autophagic activity in neurons and mice. Neuropharmacology. 2015;93:243-251.
87. Lo S, Yuan SS, Hsu C et al. Lc3 over-expression improves survival and attenuates lung injury through increasing autophagosomal clearance in septic mice. Ann Surg. 2013;257:352-363.
88. Webb JL, Ravikumar B, Atkins J, Skepper JN, Rubinsztein DC. Alpha-Synuclein is degraded by both autophagy and the proteasome. J Biol Chem. 2003;278:25009-25013.
89. Williams A, Jahreiss L, Sarkar S et al. Aggregate-prone proteins are cleared from the cytosol by autophagy: therapeutic implications. Curr Top Dev Biol. 2006;76:89-101.
90. Patil SP, Jain PD, Ghumatkar PJ, Tambe R, Sathaye S. Neuroprotective effect of metformin in MPTP-induced Parkinson's disease in mice. Neuroscience. 2014;277:747-754.

91. Crews L, Spencer B, Desplats P et al. Selective molecular alterations in the autophagy pathway in patients with Lewy body disease and in models of alpha-synucleinopathy. PLoS One. 2010;5:e9313.
92. Bai X, Wey MC, Fernandez E et al. Rapamycin improves motor function, reduces 4-hydroxynonenal adducted protein in brain, and attenuates synaptic injury in a mouse model of synucleinopathy. Pathobiol Aging Age Relat Dis. 2015;5:28743.
93. Savolainen MH, Richie CT, Harvey BK, Männistö PT, Maguire-Zeiss KA, Myöhänen TT. The beneficial effect of a prolyl oligopeptidase inhibitor, KYP-2047, on alpha-synuclein clearance and autophagy in A30P transgenic mouse. Neurobiol Dis. 2014;68:1-15.
94. Richter F, Fleming SM, Watson M et al. A GCase chaperone improves motor function in a mouse model of synucleinopathy. Neurotherapeutics. 2014;11:840-856.
95. Saxton RA, Sabatini DM. mTOR Signaling in Growth, Metabolism, and Disease. Cell. 2017;168:960-976.
96. Mihaylova MM, Shaw RJ. The AMPK signalling pathway coordinates cell growth, autophagy and metabolism. Nat Cell Biol. 2011;13:1016-1023.
97. Guo X, Farías GG, Mattera R, Bonifacino JS. Rab5 and its effector FHF contribute to neuronal polarity through dynein-dependent retrieval of somatodendritic proteins from the axon. Proc Natl Acad Sci U S A. 2016;113:E5318-5327.
98. Farías GG, Cuitino L, Guo X et al. Signal-mediated, AP-1/clathrin-dependent sorting of transmembrane receptors to the somatodendritic domain of hippocampal neurons. Neuron. 2012;75:810-823.

Legends to figures

Figure 1. Genome-wide CRISPR/Cas9 screen for the identification of autophagy genes.

(A) Live-cell imaging of H4 cells expressing GPF-mCherry-LC3B (H4-tfLC3B). Cells were incubated in the absence (control) or presence of 50 nM bafilomycin A_1 for 2 h prior to imaging. Cell edges are outlined. Scale bar: 10 μm. Insets are 3.6x magnifications of the boxed areas. (B) H4-tfLC3B cells were incubated without (control) or with 50 nM bafilomycin A_1 for 2 h, and GFP and mCherry fluorescence was measured by fluorescence-activated cell sorting (FACS). (C) H4-tfLC3B cells were incubated in regular medium (control) or amino-acid- and serum-free medium for 4 h (nutrient deprivation), and then analyzed by FACS. (D) Schematic representation of the genome-wide CRISPR/Cas9 screen. H4-tfLC3B cells were mutated with a pooled lentiviral GeCKO v2 library. Cells with high GFP/mCherry ratio were sorted and propagated; after four rounds of sorting, genomic DNA was isolated. The sequences of sgRNAs were determined by next-generation sequencing. (E) FACS analysis of cells infected with the lentiviral pool (starting population) and cells after four rounds of sorting (final sorted population). In B, C and E, the percentages of cells in the boxed areas are indicated. (F) Ranking of genes from the CRISPR/Cas9 screen based on the RRA (Robust Ranking Aggregation algorithm) score calculated using the MAGeCK method. Genes known to participate in autophagy are labeled in red; MAP1LC3B genes (*i.e.*, LC3B and LC3B2) are labeled in black; a gene not previously implicated in autophagy, UBA6, is labeled in green. The identification of LC3B and LC3B2 may be due to the synthesis of a truncated GPF-mCherry-LC3B that cannot be degraded. The genes above the horizontal dotted line were tested in the secondary screen.

Figure 2. UBA6-KO cells accumulate LC3B-I but not LC3B-II.

(A) FACS analysis of cells from the secondary screen showing enrichment of library-infected H4 cells with increased GFP fluorescence after three rounds of sorting. The percentages of cells in

the boxed areas are indicated. (B) Ranking of genes in the CRISPR/Cas9 screen based on the RRA. Genes highlighted in red were previously reported to function in autophagy. The novel autophagy regulator UBA6 is highlighted in green. (C) H4 or HeLa cells were transfected with control or either of two UBA6 siRNAs. After 48 h, cells were analyzed by SDS-PAGE and immunoblotting for LC3B, UBA6 and β-tubulin (control). In this and all other figures, the positions of the I and II forms of LC3B are indicated. (D) Quantification of the ratio of LC3B-I and -II to β-tubulin. The ratio for control siRNA was arbitrarily set at 1. Values are the mean ± SEM from three independent experiments such as that shown in C. The indicated *p*-values were calculated using a two-way ANOVA with Tukey's multiple comparisons test. (E) WT or UBA6-KO H4 cells were transfected with control plasmid or plasmids encoding MYC-UBA6 or UBA6-MYC. The cells were analyzed by SDS-PAGE and immunoblotting with antibodies to the antigens on the right. (F) Quantification of ratio of LC3B-I to β-tubulin. The ratio for the control plasmid transfection in WT H4 cells was arbitrarily set at 1. Values are the mean ± SEM from three independent experiments. The indicated *p*-values were calculated using a one-way ANOVA with Dunnett's multiple comparisons test. (G) WT and UBA6-KO H4 cells were incubated with 50 nM bafilomycin A_1 for the indicated periods prior to SDS-PAGE and immunoblotting with antibodies to LC3B and β-tubulin. (H) Quantification of the ratio of LC3B-II to β-tubulin. The ratio of WT H4 cells not treated with bafilomycin A_1 was arbitrarily set at 1. Values are the mean ± SEM from three independent experiments such as that shown in G. The indicated *p*-values were calculated using two-way ANOVA with Tukey's multiple comparisons tests. n.s.: not significant. (I) WT and UBA6-KO H4 cells were transfected with a plasmid encoding GFP-mCherry-LC3B and loaded for 16 h with Alexa Fluor 647-conjugated dextran. Cells were then analyzed by live-cell imaging. Cell edges are outlined. Scale bar: 10 μm. Insets are 4.6x magnifications of the boxed areas. (J) The ratio of autophagosomes (red-green–positive puncta) to autolysosomes (red-blue–positive puncta) was determined. Bars represent the mean

± SEM of the ratio in 20 cells from three independent experiments. In C, E and G, the positions of molecular mass markers (in kDa) are indicated on the left.

Figure 3. UBA6 participates in monoubiquitination of LC3B.

(A) WT and UBA6-KO H4 cells were incubated with 0, 20 or 50 μM MG132 for 6 h, and analyzed by SDS-PAGE and immunoblotting with antibodies to LC3B, Ub and β-tubulin (loading control). (B) The ratio of LC3B-I to β-tubulin was determined from experiments such as that in A. The ratio in WT H4 cells without MG132 treatment was arbitrarily set at 1. Bars represent the mean ± SEM of the ratio from three independent experiments. The indicated *p*-values were calculated using two-way ANOVA with Tukey's multiple comparisons tests. Other differences were not significant. (C) WT and UBA6-KO cells were transfected with plasmids encoding HA-Ub and FLAG-LC3B. Cell lysates were immunoprecipitated (IP) with antibody to the FLAG epitope, and cell lysates and immunoprecipitates were analyzed by SDS-PAGE and immunoblotting with antibodies to the HA and FLAG epitopes. (D) H4 cells were transfected with plasmids encoding HA-Ub and FLAG-LC3B. Cells were incubated with 20 μM MG132 for 6 h before lysis and immunoprecipitation with antibody to the FLAG epitope. Cell lysates and immunoprecipitates were analyzed by SDS-PAGE and immunoblotting with antibodies to the HA and FLAG epitopes. (E) Immunofluorescence microscopy showing the localization of FLAG-LC3B and FLAG-LC3B-G120A mutant in WT H4 cells. DAPI (blue) was used to stain the nucleus. Cell edges are outlined. Scale bar: 10 μm. (F) H4 cells expressing HA-Ub together with FLAG-LC3B or FLAG-LC3B-G120A mutant were analyzed by immunoprecipitation with antibody to the FLAG epitope, followed by SDS-PAGE and immunoblotting with antibodies to the HA and FLAG epitopes. (G) H4 cells were transfected with plasmids encoding FLAG-tagged Atg8-family proteins and HA-Ub. Cell lysates were subjected to immunoprecipitation with antibody to the FLAG epitope, and cell lysates and immunoprecipitates were analyzed by SDS-PAGE and immunoblotting with antibodies to the HA and FLAG epitopes. (H) H4 cells

were transfected with control or HA-Ub-encoding plasmids. Ubiquitinated proteins in the cell lysates were enriched by immunoprecipitation with antibody to the HA epitope. Cell lysates and immunoprecipitates were analyzed by SDS-PAGE and immunoblotting with antibodies to LC3B or the HA epitope. In A, C, D, G, F and H, the positions of molecular mass markers (in kDa) are indicated on the left.

Figure 4. LC3B is ubiquitinated on lysine-51.

(A) Sequence of human LC3B. Lysine residues are highlighted in red. A glycine residue that becomes conjugated to phosphatidylethanolamine is highlighted in blue. (B) and (C) H4 cells were transfected with WT and mutant LC3B constructs and HA-Ub. The ubiquitination of LC3B was examined as described for Figure 3C. (D) Binding of the LC3-interacting region (LIR) motif of SQSTM1 (DDWTHL) (stick representation) to LC3B (surface representation) (PDB code: 2ZJD). Yellow and green indicates residues involved in hydrophobic interactions; blue and red indicates residues forming hydrogen bonds. (E) H4 cells were transfected with plasmids encoding control, FLAG-LC3B or FLAG-LC3-K51R mutant plasmids. Cell lysates were immunoprecipitated with antibody to the FLAG epitope. Cell lysates and immunoprecipitates were analyzed by SDS-PAGE and immunoblotting with antibodies to SQSTM1, NBR1, NIX and the FLAG epitope. In B, C and E, the positions of molecular mass markers (in kDa) are indicated on the left.

Figure 5. BIRC6 KO increases the level of LC3B-I.

(A) H4-tfLC3B cells were mutated with a CRISPR/Cas9 lentiviral library targeting ubiquitination-related genes. The figure shows a FACS analysis of the enrichment of library-infected cells with increased GFP fluorescence after three rounds of sorting and expansion. (B) Ranking of genes based on the RRA. ATG7 (control) is highlighted in red. The novel autophagy regulators UBA6 and BIRC6 are highlighted in green. (C) H4 cells were transfected with control,

BIRC6 or UBA6 siRNAs. Cells were analyzed by SDS-PAGE and immunoblotting for LC3B, BIRC6, UBA6 and β-tubulin (loading control). (D) SDS-PAGE and immunoblotting of lysates from WT, UBA6-KO and BIRC6-KO H4 cells with antibodies to the proteins on the right. (E) Quantification of the ratio of LC3B-I and -II proteins to β-tubulin. The value of LC3B-I/β-tubulin in WT H4 cells was arbitrarily set at 1. Values are the mean ± SEM from three independent experiments such as that shown in D. The indicated *p*-values were calculated using a two-way ANOVA with Tukey's multiple comparisons test. (F) WT and BIRC6-KO H4 cells were transfected with plasmid encoding tfLC3B and allowed to internalize Alexa Fluor 647-conjugated dextran for 16 h to label late endosomes and lysosomes. GFP, mCherry and Alexa Fluor 647 fluorescence was visualized by live-cell imaging. Scale bar: 10 μm. Insets are 4.6x magnifications of the boxed areas. (G) The ratio of the number of autophagosomes (red-green–positive puncta) to autolysosomes (red-blue–positive puncta) was determined. Bars represent the mean ± SEM of the ratio in 10 cells from three independent experiments. n.s., not significant, according to an unpaired Student's *t* test. (H) WT, BIRC6-KO and UBA6-KO H4 cells were starved of amino acids and serum for the indicated periods, and analyzed by SDS-PAGE and immunoblotting with antibodies to LC3B and β-tubulin. (I) Ratio of LC3B-II to β-tubulin at different times relative to the ratio in fed WT H4 cells (set at 1). Points represent the mean ± SEM of the ratio from three independent experiments such as that in H. The indicated *p*-values were calculated using a two-way ANOVA with Tukey's multiple comparisons test. In C, D and H, the positions of molecular mass markers (in kDa) are indicated on the left.

Figure 6. UBA6 and BIRC6 function as E1 and E2/E3 enzymes, respectively, for LC3B monoubiquitination.

(A) WT, UBA6-KO and BIRC6-KO H4 cells were transfected with plasmids encoding HA-Ub and FLAG-LC3B. Cell lysates were analyzed by immunoprecipitation with antibody to the FLAG epitope, followed by SDS-PAGE and immunoblotting with antibodies to the HA and

FLAG epitopes. (B) WT H4 cells were transfected with control or FLAG-BIRC6 plasmids. Cell lysates were analyzed by immunoprecipitation with antibody to the FLAG epitope, followed by SDS-PAGE and immunoblotting with antibodies to the FLAG epitope and UBA6. (C) Plasmids encoding GFP-LC3B and FLAG-BIRC6 were transfected into H4 cells. Cell lysates were analyzed by immunoprecipitation with antibody to the FLAG epitope, followed by SDS-PAGE and immunoblotting with antibodies to the GFP and the FLAG epitope. (D) FLAG-BIRC6 immunopurified from 10^7 HEK293T cells transfected with FLAG-BIRC6 plasmid was incubated with recombinant HA-Ub, 6xHis-LC3B and GST-UBA6 in a reaction buffer containing ATP at 37°C for 30 min. Samples were analyzed by SDS-PAGE and immunoblotting with antibodies to the antigens on the right. Notice the ubiquitination of LC3B (LC3B-Ub) only when all the components are present in the mix. (E) WT and C4597A-mutant FLAG-BIRC6 were analyzed for their ability to ubiquitinate 6His-LC3B as in D. In all the panels, the positions of molecular mass markers (in kDa) are indicated on the left.

Figure 7. BIRC6 KO reduces the formation of puromycin-induced ALIS.

(A) WT and BIRC6-KO H4 cells were incubated with 100 μg/ml cycloheximide (CHX) for the indicated periods. Cells were lysed and analyzed by SDS-PAGE and immunoblotting for the proteins indicated on the right. (B,C) Quantification of the ratio of SQSTM1 (B) and NBR1 (C) to actin at different times after the addition of CHX. Values were normalized to the ratio in untreated WT H4 cells (set as 1). Values are the mean ± SEM from three independent experiments such as that shown in A. The indicated *p*-values were calculated using two-way ANOVA with Tukey's multiple comparisons test. (D) WT and BIRC6-KO H4 cells were incubated without (control) or with 5 μg/ml puromycin for 2 and 8 h. Cells were subsequently immunostained for SQSTM1 and Ub, and examined by confocal microscopy. Scale bar: 10 μm. (E) Quantification of the area (in μm^2) of SQSTM1-positive puncta determined from cells such as those shown in D. Values represent the mean ± SEM of the puncta area in 30 cells from three

independent experiments. The indicated *p*-values were calculated using two-way ANOVA with Tukey's multiple comparisons test. (F) WT or BIRC6-KO cells were transfected with control plasmid or plasmid encoding FLAG-BIRC6 as indicated in the figure, and incubated with 5 μg/ml puromycin for 4 h prior to immunostaining with antibodies to SQSTM1 and the FLAG epitope. Scale bar: 10 μm. A FLAG-BIRC6–expressing cell is outlined. (G) Quantification of the area of SQSTM1 positive puncta. Values represent the mean ± SEM of the puncta area in 30 cells from three independent experiments. The *p*-values shown in panels B, C, E and G were calculated using a one-way ANOVA with Dunnett's multiple comparisons test.

Figure 8. BIRC6 KO promotes the clearance of α-synuclein aggregates in neurons.

(A) Confocal microscopy of cultured rat hippocampal neurons co-transfected with plasmids encoding GFP-α-synuclein A53T mutant, control-mCherry or rat Birc6 shRNA-mCherry, and shRNA-resistant FLAG-tagged human BIRC6 (rescue), as indicated in the figure. Transfections were performed at 3 days-in-vitro (DIV) and neurons were fixed for immunofluorescence assay at 7 DIV. Single-channel images are shown in inverted grayscale. Arrowheads indicate α-synuclein aggregates in the axon. Scale bar: 100 μm. (B) Magnified and straightened axons from control, Birc6-KD and FLAG-BIRC6-rescue neurons shown in A. Arrowheads indicate α-synuclein aggregates in the axon. (C) Quantification of the number of α-synuclein aggregates per 100 μm of axon. Values are the mean ± SEM from 25 neurons from three independent experiments. The indicated *p*-values were calculated using a one-way ANOVA with Dunnett's multiple comparisons test. (D) Cultured rat hippocampal neurons were transfected as in A. Neurons were extracted in Triton X-100 buffer and centrifuged. Supernatants were collected as the Triton-soluble fraction, while the pellets were resuspended in 5% SDS buffer as the Triton-insoluble fraction. Fractions were analyzed by SDS-PAGE and immunoblotting with antibodies to GFP (to detect GFP-α-synuclein) and β-tubulin (loading control). The positions of molecular

mass markers (in kDa) are indicated on the left. (E) Quantification of the ratio of Triton-insoluble and -soluble GFP-α-synuclein. The value in control-shRNA–transfected neurons was set at 1. Values are the mean ± SEM from three independent experiments such as that in panel D. The indicated *p*-values were calculated using a one-way ANOVA with Dunnett's multiple comparisons test. (F) Schematic representation of the role of UBA6 and BIRC6 in LC3 ubiquitination and targeting for degradation, decreasing the amount of LC3 that can be modified with PE for its function in autophagy.

Figure 1

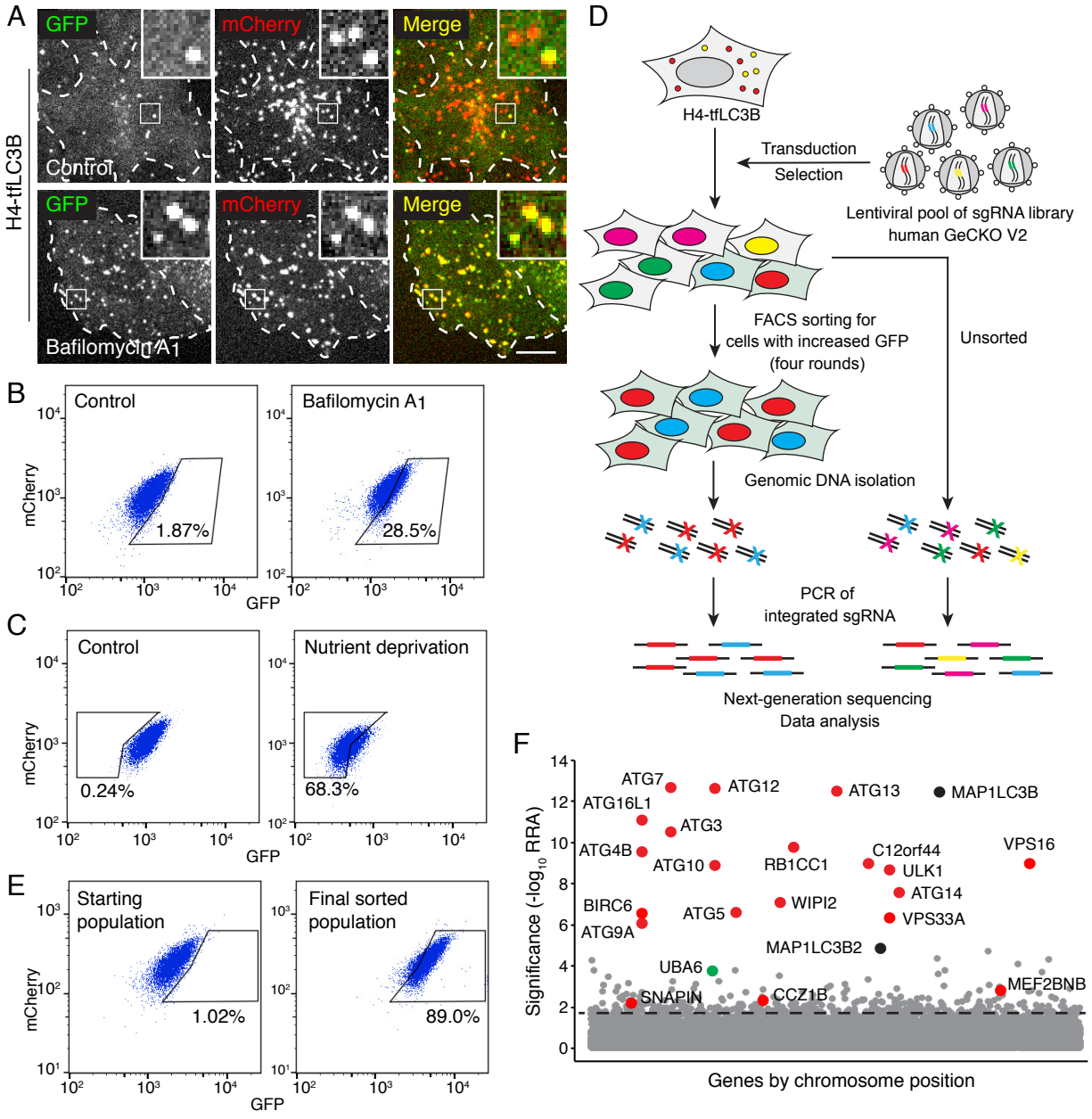

Figure 2

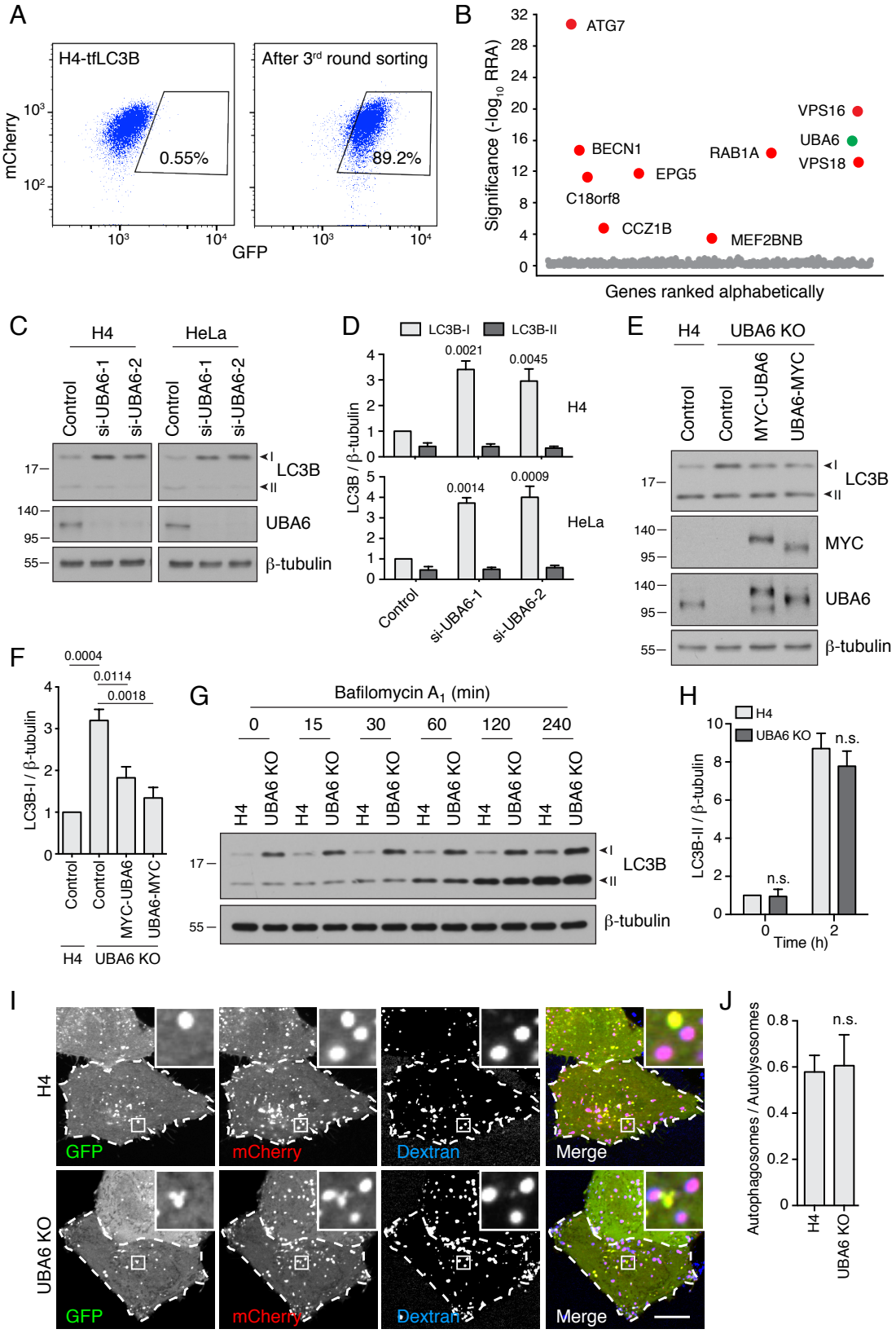

Figure 3

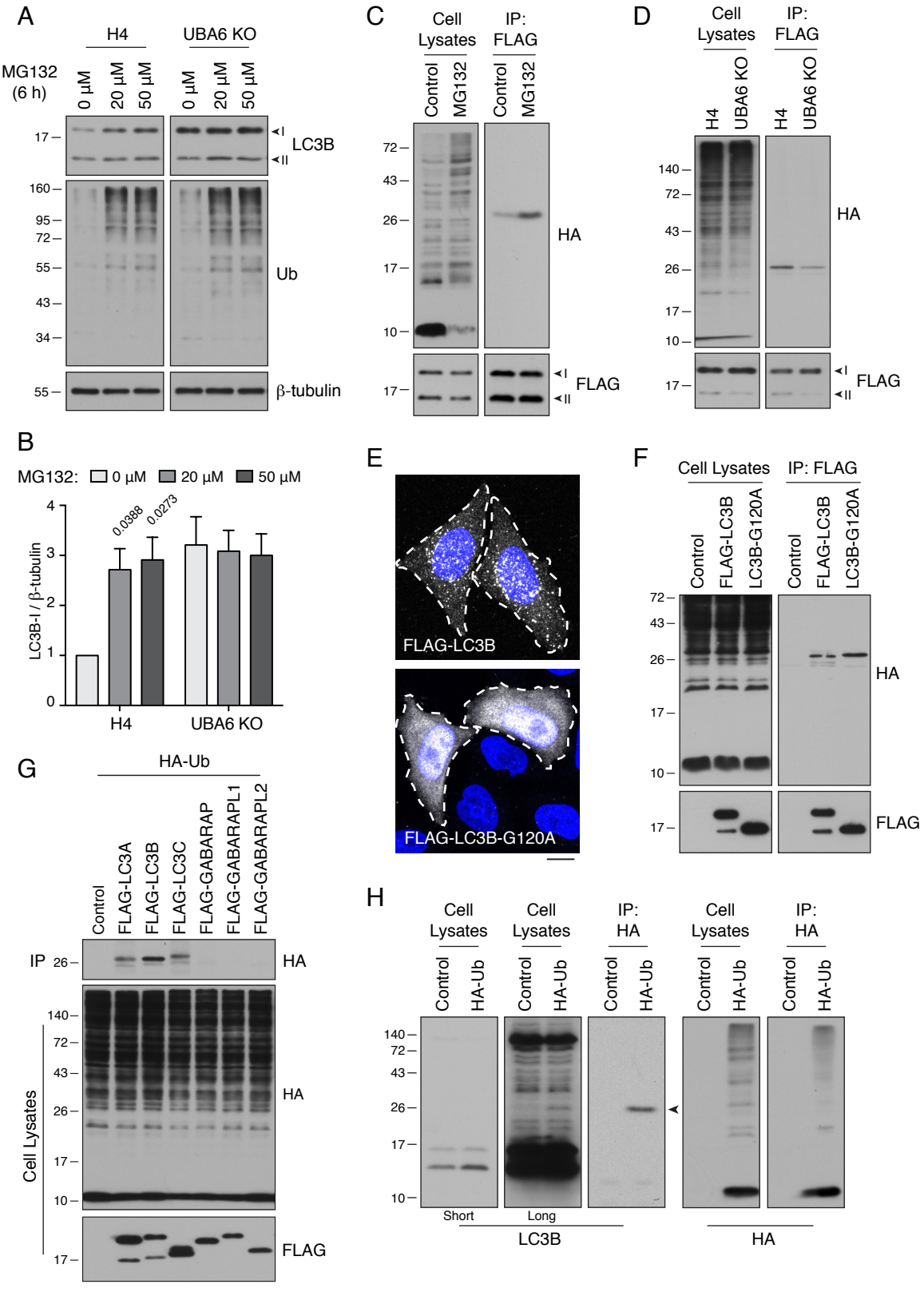

Figure 4

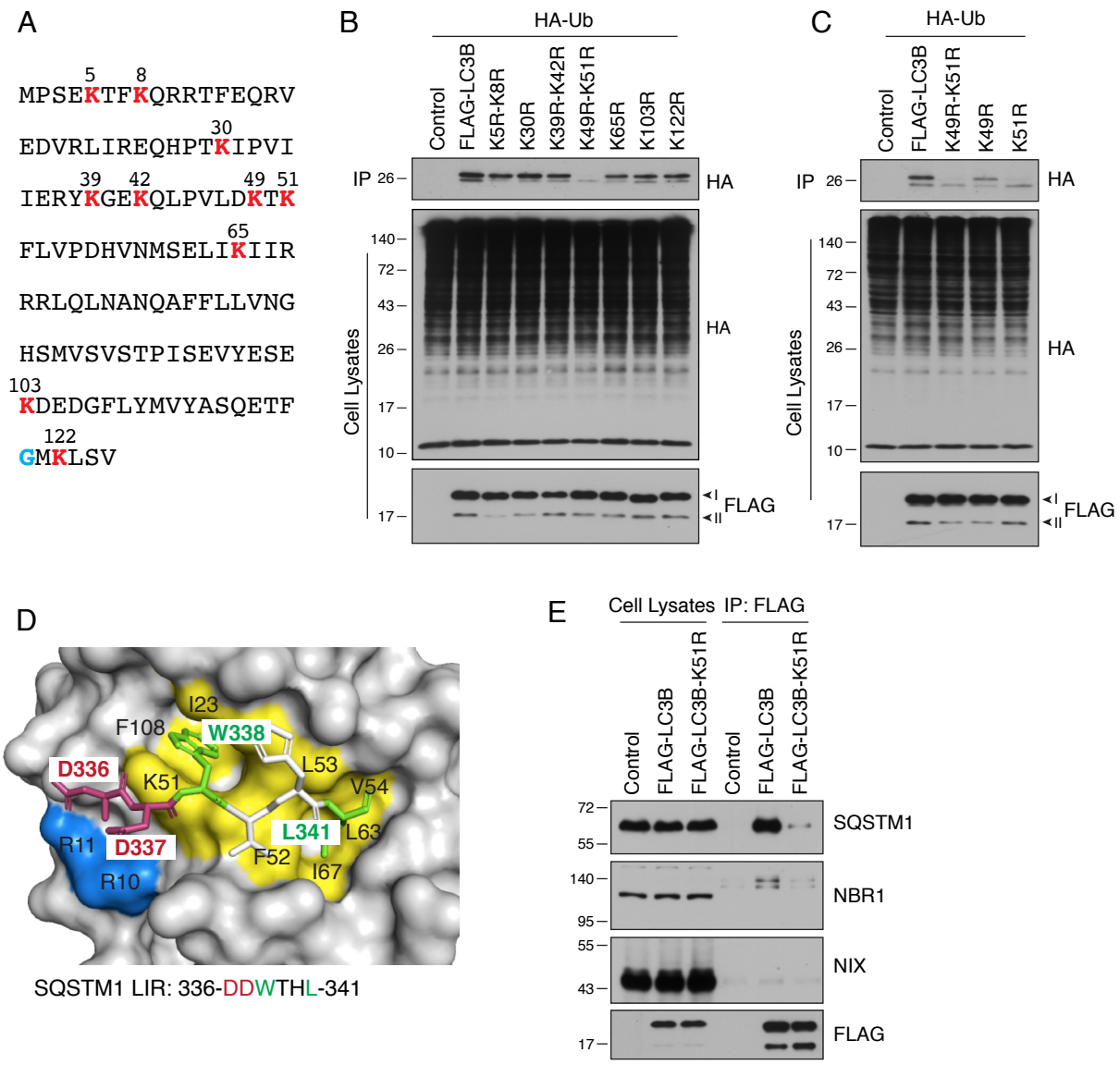

Figure 5

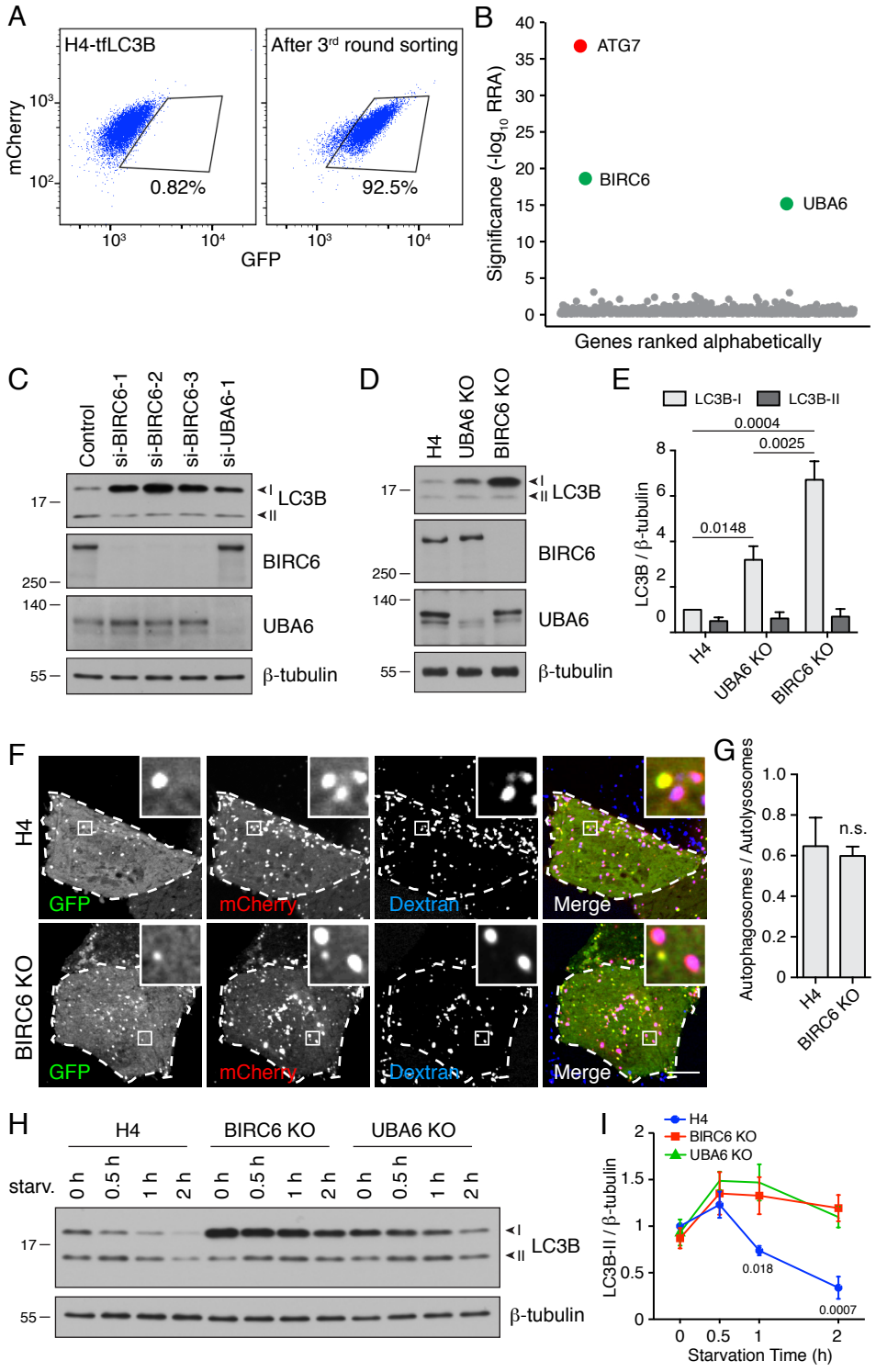

Figure 6

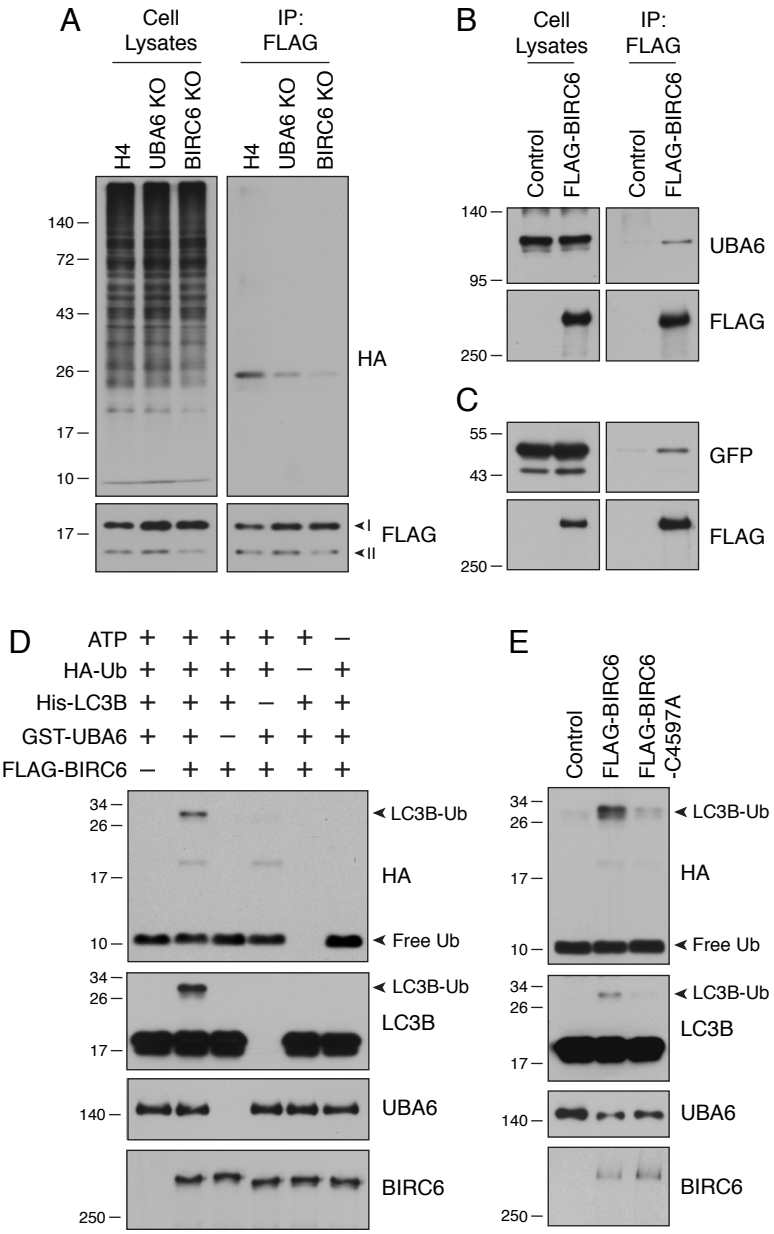

Figure 7

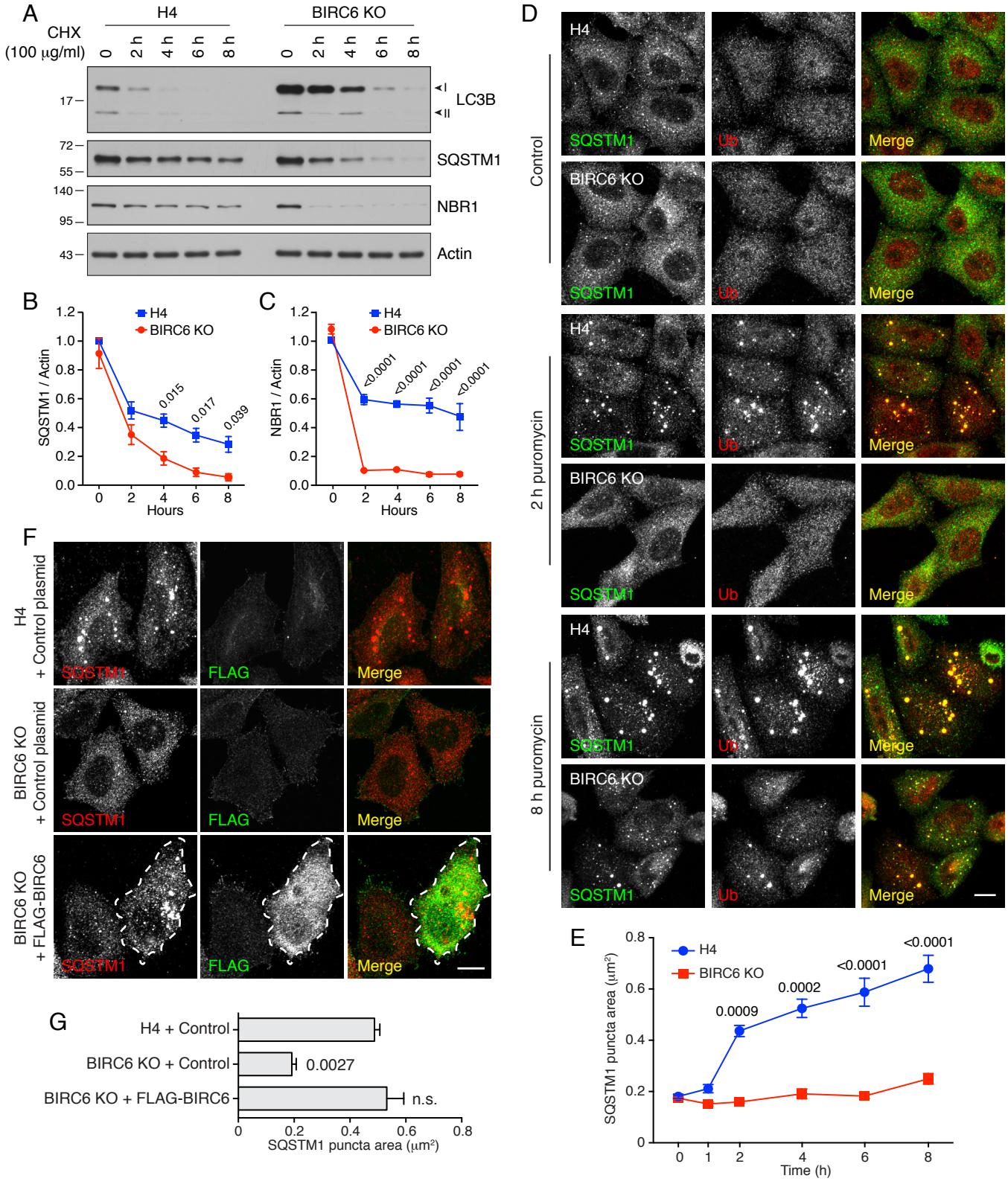

Figure 8